DOI: 10.26599/FSHW.2026.9251009

Contents lists available at SciOpen

Food Science and Human Wellness

journal homepage: https://www.sciopen.com/journal/2097-0765

China Food Publishing Co.

Fermented *Astragalus Radix* improve immune function and repair the intestinal mucosal injury in a cyclophosphamide-induced mouse model

Ze Wu[a,b,c#], Jinlan Zhang[a,b#], Longshan Zhao[c], Dandan Xu[a,b], Yan Hou[a,b], Yinghua Zhang[d], Ying Chen[d], Yun Zhang[a,b*], Zhengqi Dong[a,b*]

[a] *State Key Laboratory of Quality Ensurance and Sustainable Use of Dao-Di herbs, Institute of Medicinal Plant Development, Chinese Academy of Medical Sciences & Peking Union Medical College, Beijing 100193, China*

[b] *Key Laboratory of Bioactive Substances and Resources Utilization of Chinese Herbal Medicine from Ministry of Education, Chinese Academy of Medical Sciences & Peking Union Medical College, Beijing 100193, China*

[c] *School of Pharmacy, Shenyang Pharmaceutical University, Shenyang110016, China*

[d] *Jilin Provincial Academy of Chinese Medicine, Changchun 130012, China*

ABSTRACT: Existing studies have shown that probiotic fermentation can enhance the pharmacological activity of Chinese herbal medicines. *Astragalus Radix* (AR), a medicinal and edible herb, has rarely been reported regarding its fermentation. In this study, *Lactobacillus rhamnosus* GG (LGG) was used to ferment AR. By integrating sensory analysis, untargeted metabolomics, and evaluation of immune function and intestinal barrier integrity, we aimed to link fermentation-driven chemical remodeling with enhanced bioactivity. The results indicated that in fermented AR (FAR), the total flavonoid content increased by 23.5% ($P < 0.05$). Metabolomics analysis revealed that 208 compounds were significantly up-regulated and 485 compounds were significantly down-regulated in FAR compared with AR ($P < 0.05$), leading to significant differences in flavor between FAR and AR. Subsequently, we evaluated the intervention effects of AR and FAR in cyclophosphamide-induced immunosuppressed mice. AR and FAR significantly restored the immune organ indices, increased blood cell counts, and elevated immunoglobulin levels. Specifically, FAR increased WBC, PLT, and LYMPH counts by 147.48%, 55.76%, and 149.55%, and IgA, IgG, and IgM levels by 37.15%, 33.88%, and 45.96%, respectively (compared with the CTX group, $P < 0.05$). FAR significantly repaired the intestinal barrier, increasing the expression of ZO-1, occludin, and claudin-1 across the jejunum and colon compared to the CTX group ($P < 0.05$), with efficacy superior to AR. Furthermore, FAR suppressed intestinal inflammation by inhibiting the NF-κB pathway, effectively restoring the phosphorylation levels of p-P65 and p-IκBα to normal baseline values. In addtion, FAR reshaped the gut microbiota composition by increasing microbial richness and selectively enriching SCFA-producing and beneficial genera, such as unclassified *Lachnospiraceae*, *Blautia* and *Muribaculum*, thereby restoring the microecological balance disrupted by CTX.

Key words: Fermented *Astragalus Radix,* cyclophosphamide, immune function, intestinal health.

1. Introduction

[#] Ze Wu and Jinlan Zhang contributed equally to this work.
***Corresponding author**
yunzhang@implad.ac.cn(Y. Zhang),
zqdong@implad.ac.cn (Z.Q. Dong).

Received 16 December 2025
Received in revised from 20 January 2026
Accepted 9 February 2026

The immune system guards against foreign invasions, it can identify and eliminate antigens and works with other bodily processes to ensure health. Many factors, such as malnutrition, increased stress, immunodeficiency diseases and chemotherapy, can weaken the immunity and increase susceptibility to pathogenic microbial infections[1]. Although immune system disorders are often treated with chemical drugs, such as levamisole hydrochloride (LH) and thymosin, prolonged high doses can cause adverse reactions, such as fever, neutropenia, and allergic responses[2, 3]. Therefore, it is crucial to develop safer, effective immunomodulatory products to reduce the adverse impact of chemical pharmaceuticals and enhance the therapeutic benefits.

Taking certain functional food-medicine homologous substances can improve the body's immune status. *Astragalus Radix* (AR) is a well-known component of traditional Chinese medicine, it has attracted research attention due to its excellent pharmacological activities[4, 5]. In 2023, it was included in the list of Medicine and Food Homology substances (MHFs) by the National Health Commission of China. According to traditional Chinese medicine, AR can strengthen the spleen and elevate Qi and Yang, reflecting its potential immune-modulating properties[6]. Modern pharmacological studies have confirmed that the immunomodulatory effect is a key pharmacological feature of AR[7]. Its main active ingredients include polysaccharides, flavonoids, and saponins[8]. However, traditional preparation methods (water decoction or pieces) present certain limitations. The bioavailability of high-molecular-weight polysaccharides is relatively low[8, 9]. The main active ingredients are also present in low content such as flavonoids and saponins. The characteristic odor of AR can impart an unfavorable taste, potentially reducing user acceptance, which restricts the clinical application of AR. Therefore, employing specific methods to process AR is of great significance for enhancing its immune effects.

Probiotic fermentation technology provides a new approach for increasing the bioavailability and efficacy of the active ingredients found in medicine and food homologs[10]. Probiotics can release free aglycones by degrading traditional Chinese medicine substrate glycosides, thereby increasing the content of bioactive ingredients such as flavonoids, saponins, alkaloids, etc. It also can catabolize or convert substrates into more biologically active via enzymatic action[11]. For example, the content of flavonoids and saponins in AR are increased after fermentation, with a notable rise in the active ingredient[12].Wang et al. found that *Bacillus subtilis*-fermented AR improved hyperuricemia in mice[13]. These studies provide information on the increased activity of AR after fermentation. However, previous studies have often focused only on immune organ indicators or basic chemical changes, and people not conducted in-depth research on the immune regulatory effects and intestinal barrier repair function of FAR. In addition, the metabolomic changes and biotransformation processes of the fermentation process have not yet been determined.

LGG is a well-studied probiotic with a long history of safe use in food products. In addition, it is capable of producing carbohydrate-active enzymes (e.g., β-glucosidase/β-galactosidase), which can facilitate the biotransformation of glycosides and the remodeling of polysaccharide structures, thereby potentially enhancing the bioavailability of AR components[14, 15]. This study aims to provide an AR beverage fermented

by LGG, and we evaluate its performance through a comprehensive approach that combines sensory analysis, metabolomics, and multi-level biological assessment. We sought to concurrently examine how fermentation-induced metabolic remodeling contributes to immune recovery. This includes evaluating its effects on immune organ restoration, repair of intestinal tight junctions, regulation of the NF-κB pathway, and recovery of the gut microbial community.

2. Methods and materials

2.1 Materials

The AR was acquired from Yulin City, Shaanxi Province, China (60 months), while the LGG (ATCC 53103, LGG) was obtained from Chr Hansen (Hørsholm, Denmark). The fetal bovine serum and cell counting kit-8 were supplied by Gibco Life Technologies (Waltham, MA, USA) and Beyotime Biotechnology Co. Ltd. in Shanghai (China), respectively. The ELISA kits for the detection of IgA, IgG, and IgM, as well as the lymphocyte (LYMPH) separation kit and De Man-Rogosa-Sharpe (MRS) medium, were provided by Solarbio Science and Technology Co. Ltd. in Beijing (China). The antibodies for Western blot analysis, including those against β-actin, ZO-1, occludin, claudin-1, P65, IκBα, p-P65, and p-IκBα, were all purchased from Proteintech Group (Wuhan, China). All other reagents were chromatographic and analytical grade.

2.2 AR and FAR preparation

According to the decoction method used in traditional Chinese medicine, the AR powder (65 mesh) was soaked in 10-fold distilled water and subjected to two cycles of heating and reflux, each lasting 90 min. The filtrates were mixed and condensed at 50℃ using a vacuum rotary evaporator. The resulting AR extract, equivalent to 166.67 mg/kg of the crude drug, was subjected to a 10 min centrifugation at 3,000×g and 4℃ and sterilized at 121℃ for 20 min.

LGG was isolated and cultured by streaking on MRS medium containing 2% agar to purify the bacterial strain. After 24 h, the colonies were selected and further enriched in the MRS liquid medium. The bacterial solution concentration was adjusted to 1.0×10^8 CFU/mL. Based on the results of preliminary experiments, the probiotic was injected into the AR extract at a 1% (v/w) inoculation rate, after which the mixed system was fermented at 30℃ for 24 h. Next, the number of viable LGG bacteria was measured using the plate coating counting method. FAR were heated at 100℃ for 30 min to stop the fermentation reaction. AR was prepared using the same method without adding LGG. The samples were centrifuged at 4℃ and 8,000×g for 15 min to obtain the supernatant, which was divided into two portions. One portion was frozen and stored at -80℃, while the other was lyophilized and stored at -80℃ for further research.

2.3 The main active substances in the AR and FAR

2.3.1 Polysaccharide content determination

The phenol-sulfuric acid technique was employed to determine the total polysaccharide level[16]. 4 g of AR and FAR lyophilized powder was extracted twice with 40 mL water for 1.5 h at 90℃. The combined filtrates were condensed to 35 mL, mixed with 50 mL of 95% ethanol for overnight precipitation, and

centrifuged. The polysaccharide precipitate was dried at 40°C and redissolved in 50 mL of water. Then, 2 mL aliquots were blended with 5 mL concentrated sulfuric acid and 1 mL of a solution containing 5% phenol, heated in boiling water for 15 min, and cooled, followed by absorbance measurements at 490 nm, with D-anhydrous glucose (10 to 100 μg/mL) as the standard.

2.3.2 Determination of the total flavonoids

Here, 1 g of AR and FAR powder was reflux-extracted with 20 mL 70% ethanol at 70℃ for 3 h, compensating for any weight loss. Next, 1 mL filtrate was combined sequentially with 0.5 mL 5% $NaNO_2$ for 6 min and 0.5 mL of 10% $Al(NO_3)_3$ for 6 min, and 4 mL 1M NaOH. This mixture was diluted with ethanol for spectrophotometric measurement at 500 nm, using a 70% ethanol blank and a rutin standard curve for quantification[17].

2.3.3 Determination of the total saponins

The total saponins were extracted and quantified using previously delineated methods[18]. Briefly, 1 g of lyophilized AR and FAR powder was obtained twice at 70℃ using 10 mL 70% ethanol. The combined filtrates were concentrated to 2 mL, segregated using water-saturated n-butanol, and evaporated. This was followed by residue dissolution in methanol to 25 mL, after which 0.5 mL aliquots were mixed with perchloric acid (0.8 mL) and 5% vanillin-acetic acid (0.2 mL) for a 15-min reaction at 60℃. The solution was cooled using ice and combined with 5 mL of acetic acid for spectrophotometric measurement at 540 nm, using astragaloside IV standards for calibration.

2.4 Sensory analysis

2.4.1 Electronic tongue analysis

Here, 10 mL of AR and FAR were combined with 200 mL deionized water, boiled for 20 min, and filtered, followed by 10-min centrifugation at 10,000×g to acquire the supernatant. The prepared sample decoction was passed through a microporous 0.45 μm membrane, after which 100 mL of the filtrate was transferred to a designated electronic tongue beaker. The electronic tongue was equipped with seven independent sensors (AHS, PKS, CTS, NMS, SCS, CPS, and ANS), which were activated, calibrated, and diagnosed before testing to ensure stability. The "sample - water - sample" sequence was followed and the sensors were cleaned thoroughly after each test to avoid cross contamination. The sensor probe was inserted into the sample to initiate the testing process. Each sample was tested six times, with a data collection time of 120 s for each sample. One data point was collected per second, and the stable response signal collected between 100 s and 120 s was used as the output value.

2.4.2 Electronic nose analysis

The electronic nose information was evaluated utilizing a technique delineated by Yao et al[19]. Here, 2 mL of AR and FAR were placed in injection bottles and incubated at 50℃ for 15 min, followed by headspace injection. The analysis parameters included clean air as the carrier gas, a sample injection detection time of

120 s, an internal flow rate of 300 mL/min, and data collection intervals of 100 s and 105 s. Each sample was measured in parallel five times.

2.5 Untargeted metabolomics analysis

According to a previously delineated method[20], to extract the metabolites, 200 μL each of AR and FAR were mixed with 800 μL of a methanol:acetonitrile (1:1, v/v) solution. This was followed by vortexing for 30 s, sonication at 4℃ and 40 Hz for 30 min, incubation for 30 min at -20℃, and a 10 min, 4℃ centrifugation at 13,000×g. A Thermo UHPLC-Q Exactive system from Thermo Fisher Scientific (MA, USA) was used for supernatant processing. Mobile phase A contained 2% acetonitrile-water and 0.1% formic acid, while mobile phase B comprised acetonitrile and 0.1% formic acid, which were delivered at 0.40 mL/min using a 100 mm×2.1 mm i.d., 1.7 μm ACQUITY BEH C18 column (Waters, USA) at 40℃ and an injection volume of 5 μL. The MS conditions included a 450℃ ion source temperature, 20-40-60 V cyclic collision energy, 70 m/z to 1050 m/z mass range, 3,500 V positive ion voltage, -3,000 V negative ion voltage, 50 arb sheath gas, 13 arb Aux gas flow rate, 70,000 MS resolution, and 17,500 MS/MS resolution. Both negative and positive ion modes were used to obtain the MS signals of the samples in a 70 m/z to 1050 m/z scanning range. The raw information was processed with Progenesis QI, while the metabolites were identified against the TCM metabolite database (MJBIOTCM) at Majorbio Biotechnology Co. Ltd. (Shanghai, China). Approximately 80% of the characteristic metabolic components identified in the sample groups were retained, followed by data filling and normalization. The "ropls" R package was used for principal component analysis (PCA), while metabolites showing VIP>1 and $p<0.05$ exhibited significant differences. The metabolic and pathway enrichment was analyzed using the KEGG database (http://www.genome.jp/kegg/), while MetaboAnalyst was employed to map the metabolite differences to the corresponding biochemical pathways.

2.6 Animal assay

2.6.1 Group administration

The Animal Ethics Committee of the Institute of Medicinal Plant Development, Chinese Academy of Medical Sciences (Approval No. SLXD-20240905019) approved all the experimental procedures. Due to the immune-enhancing effect of estrogen and to avoid the impact of cyclical fluctuations in estrogen and progesterone on the experimental outcomes, this study exclusively used male BALB/c mice between six and eight weeks old with initial body weights between 20 g- 22 g, supplied by Beijing SPF Biotechnology Co. Ltd. The mice were acclimatized for 5 d in specific pathogen-free (SPF) conditions at 25 ± 2℃, 50% to 60% humidity, and a 12 h/12 h light/dark cycle, providing free access to water and food. Next, the mice were segregated randomly into five groups (n = 6 per group): Control, CTX, AR, FAR, and positive control (LH).

With the exception of the Control, the remaining groups were injected intraperitoneally with CTX at 80 mg/kg from 1 d to 3 d to establish an immunosuppression model[21]. From 4 d to 13 d, the control and CTX groups were orally gavaged with 0.2 mL of saline per day, while the LH mice received 40 mg/kg/d of LH[22]. The AR and FAR groups were given AR and FAR, respectively, at a crude drug dosage of 2 g/kg/d. The mouse dosage of the AR was converted from the clinical human dose based on equivalent body surface

area[13]. At 14 d, blood, spleen, thymus, jejunum, colon, and fecal samples were collected after sacrifice using isoflurane.

2.6.2 Weight, spleen index, and thymus index

The weights of the individual mice were recorded daily, and they were euthanized after the experiment. The thymus and spleen were weighed, and the immune organ index was calculated.

Thymus index = thymus weight / body weight (mg/g)

Spleen index = spleen weight / body weight (mg/g)

2.6.3 Blood cell content

Collect 100 μL of blood from the orbit of mice into a Na_2EDTA tube, gently invert it 8 to 10 times until it is fully anticoagulated, and analyze it within 24 h. According to the manufacturer's instructions, calibrate/perform quality control daily, and then operate the Mindray BC-5130 Vet fully automatic blood analyzer in mouse mode. The measured parameters include white blood cells (WBC), red blood cells (RBC), hemoglobin (HGB), platelets (PLT), and lymphocytes (LYMPH)[23].

2.6.4 The IgA, IgM, and IgG content

The blood collected from the mice were left at ambient temperature for 1 h to 2 h, followed by 15 min, 4℃ centrifugation at 3,500 rpm to collect the upper serum layer. An enzyme-linked immunosorbent assay kit was employed to determine the IgA, IgG, and IgM levels in the serum immunoglobulin.

2.6.5 LPS-induced B-LYMPH proliferation

Due to the significant decrease in the spleen index and low splenic LYMPH content after CTX modeling, two spleens were selected from each group for measurement. The mouse splenic LYMPHs were obtained using the appropriate isolation kit.

A method delineated by Dai et al[24]. was used to resuspend the spleen LYMPHs in RPMI-1640 medium with 1% P/S, 10% FBS, and 1% L-glutamine. After altering the cell concentration to 3×10^6/mL, it was placed in a 96-well plate (100 μL/well), with three wells in each group used as the control. LPS was added to the other three wells until reaching an ultimate concentration of 20 μg/mL. An equal amount of serum-free RPMI-1640 medium was introduced into the control wells, followed by 72 h cell incubation at 37℃ in a moist environment with 5% CO_2. This was followed by a 4 h incubation with 10 μL of CCK8 reagent per well and absorbance measurements at 450 nm.

The B cell proliferation rate = $A_{LPS} / A_{Control} \times 100\%$

2.6.6 Concanavalin A (ConA) induced T-LYMPH proliferation activity

The spleen cells were prepared via resuspension in RPMI-1640 medium with 1% P/S, 10% FBS, and 1% L-glutamine. The volume was adjusted 3×10^6/mL and placed in a 96-well plate (100 μL/well), with three wells in each group used as a control. ConA was introduced into the other three wells to an ultimate concentration of 10 μg/mL. An equal amount of serum-free RPMI-1640 medium was incorporated into the control wells and incubated at 37℃ for 72 h in a moist environment containing 5% CO_2. Next, 10 μL of CCK8

reagent was introduced into the individual wells and incubated for 4 h, followed by absorbance measurements at 450 nm.

The T cell proliferation rate = $A_{ConA}/A_{Control} \times 100\%$

2.6.7 Alcian blue (AB)-periodic acid-Schiff (PAS) and hematoxylin-eosin (HE) staining

Using a previously described method[25], the spleen, jejunal, and colonic tissues were fixed with 4% paraformaldehyde (PFA) and sectioned using a microtome (Leica RM2255 Co. Ltd., Germany). Next, HE, AB, and PAS were used for sample staining to assess their histomorphology, while an optical microscope (Nikon DS-RI2 Co., Ltd., Japan) was employed to obtain images.

2.6.8 Immunohistochemical evaluation

The immunohistochemical analysis was performed using a previously delineated technique[26]. The jejunal and colonic tissues were fixed with 4% PFA, embedded, and sectioned. The antigen-treated sections were sealed and incubated overnight at 4℃ with CD4+, CD8+, claudin-1, occluding, and ZO-1 primary antibodies. The secondary antibodies were added and incubated. The cell nuclei were stained using the DAB staining method, dehydrated, and mounted for slide preparation, while photos were obtained with a microscope.

2.6.9 Western blot

A previously described technique to extract the proteins from the intestinal tissues[27]. The frozen jejunal and colonic tissues were collected and homogenized with a nine-fold volume of RIPA lysis buffer consisting of a 1% phosphatase inhibitor and a 1% protease inhibitor, followed by thorough mixing in a bath with ice-water. The mixture was left to stand and incubated on ice for 30 min, respectively, to obtain the supernatant, after which the protein level was measured using BCA. Equal protein quantities were combined with loading buffer and denatured via heating. SDS-PAGE was employed for protein segragation, which were placed on PVDF membranes and blocked with 5% skim milk in TBST. This was followed by washing with TBST, overnight incubation with the primary antibodies, and rinsing and incubation using the secondary antibodies. A Bio-Rad imaging system was employed for protein band identification, while ImageJ software was utilized for quantification.

2.6.10 Gut microbiota analysis

Total genomic DNA was obtained from the feces of the mice to analyze the intestinal microbiota[28]. The DNA integrity was verified via agarose gel electrophoresis, while a NanoDrop 2000 spectrophotometer from Thermo Fisher Scientific in the USA was employed to measure the specific levels and purity. PCR was employed to enhance the hypervariable V3-V4 areas of the 16S rRNA gene, with the extracted DNA serving as a template, and using the 806R (5'-GGACTACHVGGGTWTCTAAT-3') and 338F (5'-ACTCCTACGGGAGGCAGCA-3') primers. PCR was performed in 2% agarose gel, while Synergy HTX (Biotek, USA) was employed for quantification. The pure PCR products were pooled in equimolar quantities, followed by paired-end sequenced using an Illumina NextSeq 2000 PE300 platform (Illumina, San Diego,

USA), while the QIIME 2 pipeline (version 2023.5) was used to process the quality-filtered, assembled sequences. A naive Bayes classifier in QIIME 2, trained against the SILVA 16S rRNA gene database (v138.2), was employed for the taxonomic assignment of the representative ASV sequences, while the Majorbio Cloud Platform (https://cloud.majorbio.com) was used for the bioinformatic assessment of the gut microbiota.

2.7 Statistical assessment

The experiments were performed between three and six times. The results were illustrated as the mean ± standard error. The Origin software was used for data plotting, while the SPSS software was employed for variance analysis. $P < 0.05$ denoted significant differences.

3. Results

3.1 Modifications in the levels of the main AR components

Fermentation end points were determined based on the growth dynamics of LGG in AR. The changes in the total flavonoid, saponin, and polysaccharide levels before and after fermentation were evaluated. As shown in **Table. 1**, the FAR group exhibited a decline in the total polysaccharide content, possibly due to their consumption and metabolism by LGG as carbon sources during fermentation. However, the total flavonoid levels increased by 23.5% compared to AR. This is consistent with the research of Wang et al[29]. Therefore, LGG fermentation promoted the release of AR components, which enhanced its pharmacological efficacy.

Table 1. The contents of the primary chemical components AR and FAR, determined by quantitative chemical analysis and calculated based on the dry weight (g / 100 g), were expressed as mean ± SD (n = 3). *** indicates $P < 0.001$, suggesting an extremely significant difference between the AR and FAR groups.

Bioactive components	AR	FAR
Total polysaccharide	8.49 ± 1.76%	7.16 ± 0.51%
Total saponin	3.08 ± 0.23%	3.24 ± 0.39%
Total flavone	0.98 ± 0.02%	1.21 ± 0.02%***

3.2 Sensory analysis

3.2.1 Electronic tongue

Probiotic fermentation typically alters the material basis of substrates, leading to significant sensory changes in food. An electronic tongue was employed for AR and FAR analysis to explore the flavor quality of the FAR, while the volatile substances were separated to obtain the chromatographic peaks and integral values. Next, PCA analysis was conducted (**Fig. 1A)**. The first principal component (PC1) represented 89.45% of the sample information, while the second principal component (PC2) represented 10.01%. These two principal components offered a combined variance contribution of 99.46%, fully reflecting the overall state of the sample. A significant distinction was evident between the AR and FAR groups, with notable sample concentration in each group. Furthermore, PLS-DA analysis yielded similar results (**Fig. 1B**), confirming that LGG fermentation significantly altered the AR flavor. The radar chart results (**Fig. 1C**) showed that the ANS and CTS sensors were mainly responsible for the differences between FAR and AR,

with FAR exhibiting increased sweetness and bitter flavors. In addition, FAR showed a stronger response than AR in the CTS sensor, indicating an increase in salty taste.

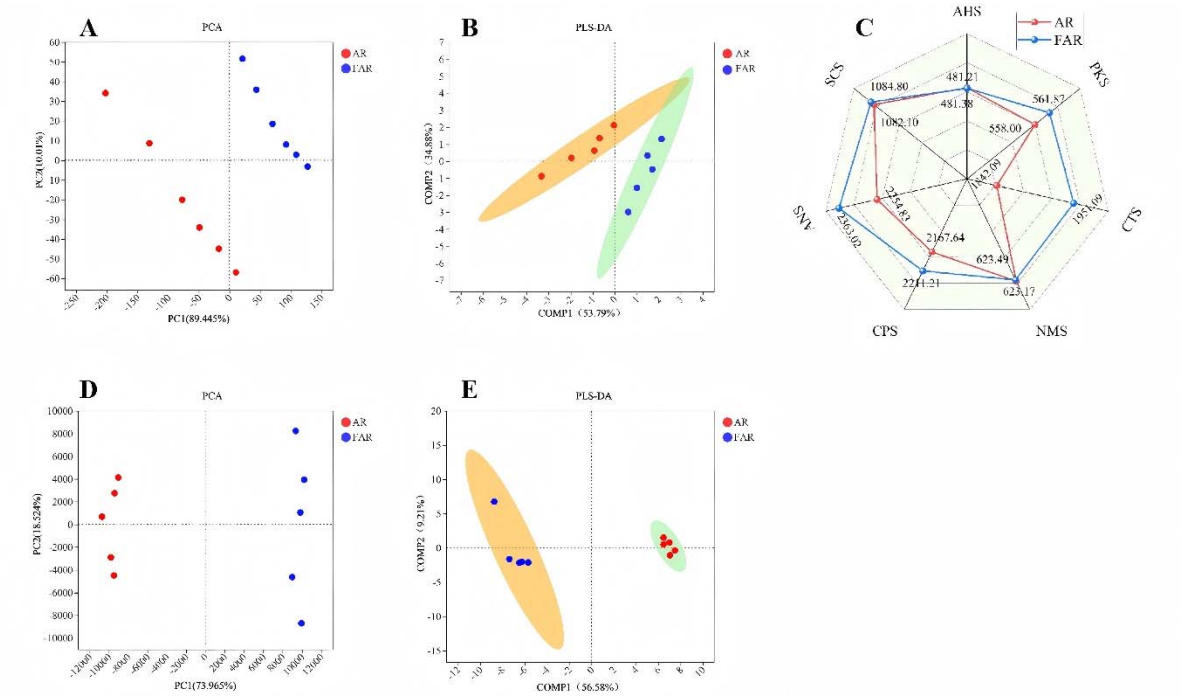


Fig. 1 Food sensory analysis of AR and FAR. (A) PCA analysis of electronic tongue. (B) PLS-DA analysis of electronic t0ongue. (C) Radar analysis diagram of electronic tongue. (D) PCA analysis of electronic nose. (E) PLS-DA analysis of electronic nose. AHS, PKS, CTS, NMS, CPS, ANS, SCS represent seven different sensors of the electronic tongue, respectively.

3.2.2 Electronic nose

Furthermore, the volatile components in the AR and FAR were measured using an electronic nose, while the differences were determined via PCA and PLS-DA **(Fig. 1D)**. PC1 reflected 73.97% of the sample information, while PC2 represented 18.52%. The cumulative variance contribution of the two principal components was 92.49%, which fully accounted for the sample information. The AR and FAR showed notable clustering within the samples, with significant separation between the groups. This confirmed the significant odor differences between the AR and FAR, which were consistent with the PLS-DA results **(Fig. 1E)**.

3.3 Metabolomic changes during LGG fermentation

Untargeted metabolomics was employed to determine the metabolite variation in the AR and FAR, while PCA was utilized to assess the metabolic profile variations pre- and post-fermentation. PC1 and PC2 denoted 53.90% and 20.80%, respectively, of the overall variance in positive ESI mode **(Fig. 2A)**, and 53.50% and 22.10% in negative ESI mode **(Fig. 2B)**. Four samples from the same group displayed close clustering, clearly distinguishing between the fermented and original samples. The findings indicated substantial variation between the AR metabolites before and after fermentation. The differential metabolites were screened by subjecting the OPLSDA VIP values to multivariate analysis, which combined the VIP value (≥ 1 and $P < 0.05$) and a fold change of difference (FC) value (≥ 1). A volcano plot was created of the sample data from the FAR and AR groups. A total of 693 significantly different metabolites were identified **(Fig. 2C)**, of which 208

were upregulated, and 485 were downregulated. The differential comparison results are presented in **Supplementary Table S1**. According to the Human Metabolism Database (HMDB), https://www.HMDB//hmdb.ca), the identified differential metabolites were divided into lipids and lipid-like substances (25.85%), organic acids and derivatives (20.13%), phenylpropanes and polyketones (14.62%), heterocyclic organic compounds (12.92%), organic oxygen-containing compounds (11.23%), and benzenes (7.84%) **(Fig. 2D)**. The 30 most abundant differential metabolites were selected for further cluster heatmap analysis **(Fig. 2E)**. The differential metabolites were mainly concentrated in carboxylic acids and derivatives, fatty acyls, flavonoids, isoflavonoids, and pyridines and their derivatives. The results showed that the flavonoid and isoflavonoid levels increased, while those of carboxylic acids and their derivatives, as well as pyridines and their derivatives, declined. Furthermore, 693 differential metabolites were entered into the KEGG database for pathway enrichment assessment **(Figs. 2F and 2G)**. The main enriched pathways of the upregulated metabolites included isoflavonoid, flavonoid, flavone, and flavonol biosynthesis, as well as linoleic acid and nucleotide metabolism. The primary enriched pathways of the downregulated metabolites included phenylalanine, tyrosine, tryptophan, pantothenate, and CoA, and betalain biosynthesis, as well as alanine, aspartate, glutamate, phenylalanine, and vitamin B6 metabolism.

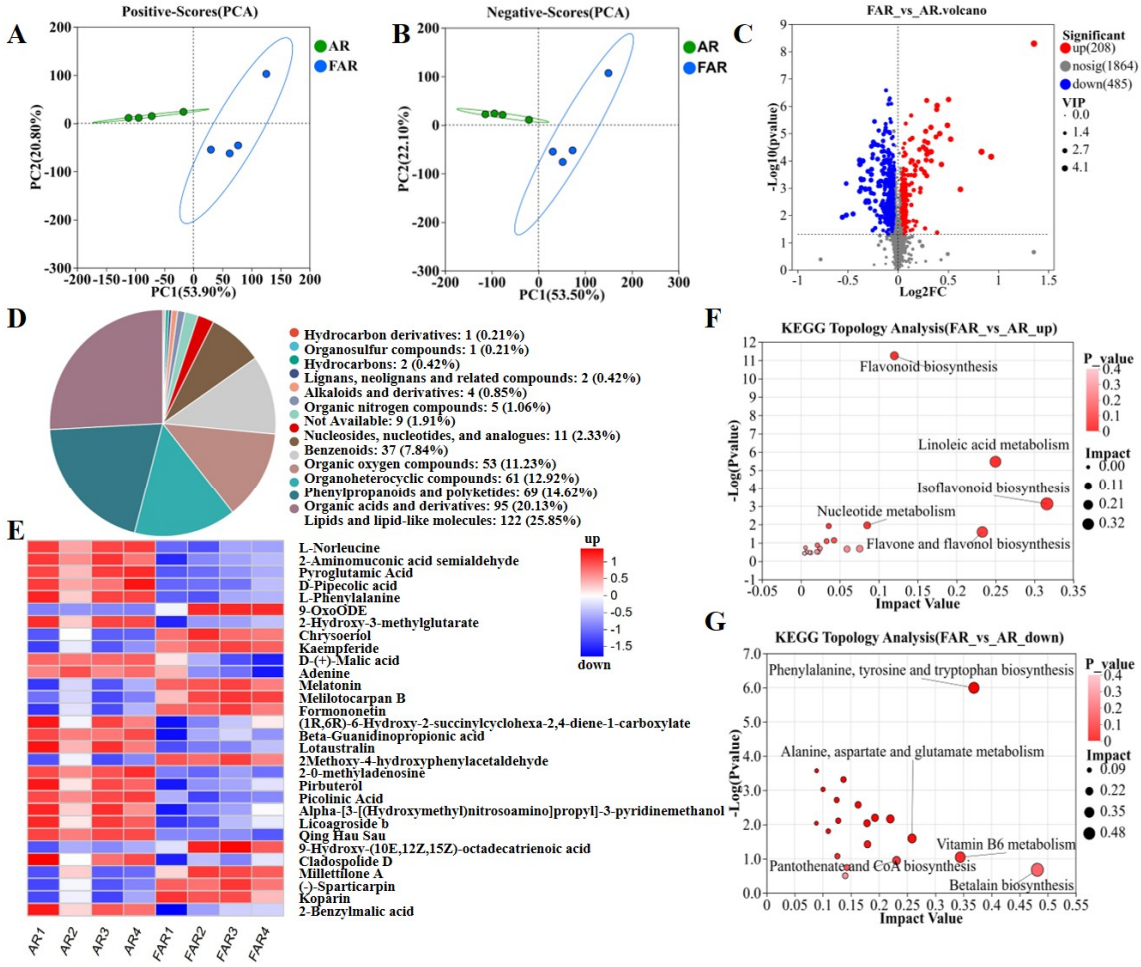


Fig. 2 Untargeted metabolomics analysis demonstrating the effects of fermentation on the metabolites of Astragalus radix. (A) PCA score plots of metabolites in positive mode; (B)PCA score plots of metabolites in negative mode; (C) Volcano plots displayed up-regulated and down-regulated metabolites; (D) Classification of the differential metabolites; (E) Cluster analysis of the top 30 differential metabolites based on HMDB; (F)Bubble plots for and annotation and enrichment of the top 20 KEGG pathway for differential metabolites; (F) FAR vs AR up-regulated and (G) FAR vs AR down-regulated metabolites.

3.4 Animals

3.4.1 Weight, thymus index, and spleen index

Fig. 3A shows the grouping and treatment of the animals. The weights of the mice, along with their spleen and thymus indexes, were measured to assess their living conditions and functional immune organ status **(Fig. 3B-C)**. After intraperitoneal CTX injection, the CTX group displayed varying degrees of weight loss, as well as lower thymus and spleen indices in comparison with the Control group ($P < 0.05$). Gavage with AR and FAR caused considerable body weight recovery relative to the CTX mice, with the weights of those in the FAR group exceeding those in the AR group, consequently alleviating the weight loss caused by CTX. As the primary lymphatic organ in the body, the thymus is crucial for T cell differentiation and maturation, while the spleen serves as a storage site for mature B and T cells. CTX, a chemotherapeutic drug and immunosuppressant, exhibits various immunosuppressive effects in mouse experiments, particularly by reducing the thymus and spleen indices, consequently weakening the nonspecific immune ability of mice[30]. The spleen and thymus atrophy caused by CTX were reversed in both the AR and FAR groups ($P < 0.05$), restoring them to near normal levels. Furthermore, the statistical results indicated that FAR improved the spleen and thymus indices compared to AR ($P < 0.01$), demonstrating that LGG fermentation enhanced AR immune activity.

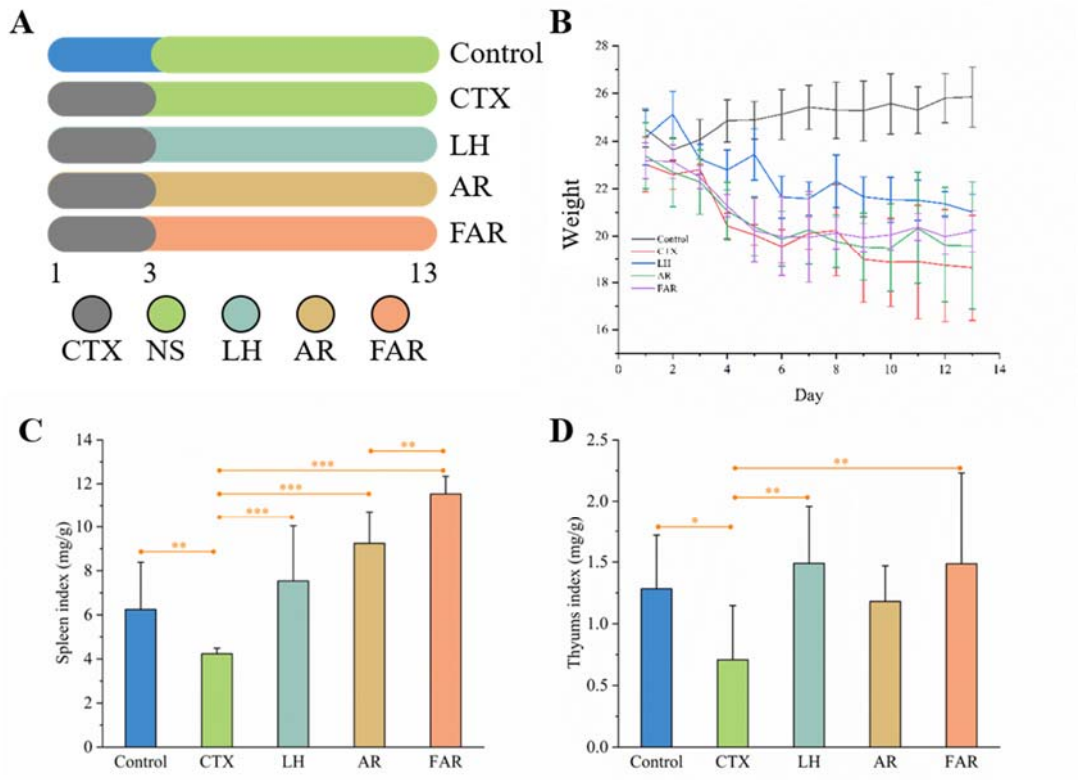


Fig. 3 Animals grouping, weight, and immune organ index. (A) Method of drug administration in mice. (B) Weight. (C) Spleen index. (D) Thymus index. (n=6). * $P < 0.05$, ** $P < 0.01$, *** $P < 0.001$.

3.4.2 Blood cell content

CTX exhibits a strong bone marrow suppressive effect, which can decrease the whole blood cell count, especially WBC, consequently increasing the risk of infection. In addition, it can significantly inhibit

LYMPH, leading to severe cellular and humoral immune dysfunction in the body. The various CTX indicators, including WBC, RBC, HGB, PLT, and LYMPH **(Table. 2)** exhibited substantially reduced levels relative to the Control group. The various indicators of CTX, especially the levels of white blood cells and lymphocytes, were significantly reduced compared to the control group. The FAR group showed an increase of 147.48%, 4.58%, 2.82%, 55.76%, and 149.55% in WBC, RBC, HGB, PLT, and LYMPH, respectively, compared to the CTX group. Compared with the AR group, the FAR group showed a more significant increase in WBC and LYMPH levels ($P < 0.05$).

Table 2. Blood cell count. WBC: white blood cell; RBC: red blood cell; HGB: hemoglobin; PLT: platelet; LYMPH: lymphocyte. $P < 0.05$ was considered statistically significant; * indicates $P < 0.05$ compared to the CTX group; ** indicates $P < 0.01$ compared to the CTX group; *** indicates $P < 0.001$ compared to the CTX group; # indicates $P < 0.05$ compared to the AR group. (n=5)

	WBC (10^9/L)	RBC (10^{12}/L)	HGB (g/L)	PLT (10^9/L)	LYMPH (10^9/L)
Control	11.5±1.43***	10.27±0.48*	155.80±7.36*	1320.2±158.00***	8.58±1.27*
CTX	4.76±1.92	9.39±0.29	142.00±5.29	822.40±108.46	4.40±0.98
LH	8.57±2.30*	9.52±0.33	146.40±5.13	1056.80±108.70	7.74±1.74*
AR	7.23±1.76	9.85±0.50	149.40±8.17	1176.20±187.54**	9.06±3.56**
FAR	11.78±3.81***#	9.82±0.41	146.00±6.04	1281.00±305.52***	10.98±3.41***

3.4.3 IgA, IgG and IgM

Immunoglobulin, produced by plasma cells differentiated from B LYMPHs, can recognize and specifically bind antigens to help the body resist pathogenic invasion. CTX can inhibit the proliferation and activation of B LYMPHs and weaken the specific immune response of the body. Therefore, the immunoglobulin content is crucial to the immune state of the body. An ELISA kit was employed to determine the immunoglobulin. The levels of IgA, IgG, and IgM antibodies were significantly lower in the CTX group than in the control group ($P < 0.001$) **(Fig. 4A-C)**, indicating successful modeling, and this is consistent with previous reports[21, 24]. After oral administration of AR or FAR, the levels of IgA, IgG, and IgM in the serum were significantly increased ($P < 0.01$), In comparison with the CTX group, AR increased IgA, IgG, and IgM by 24.25%, 35.15%, and 23.90% respectively, while FAR increased IgA, IgG, and IgM by 37.15%, 33.88%, and 45.96% respectively. And FAR group significantly increased IgM levels compared to AR group ($P < 0.05$).

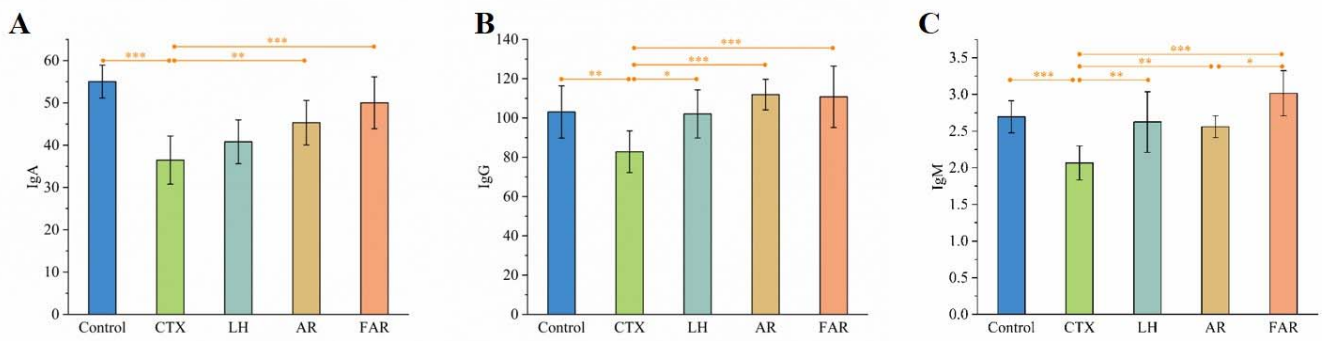


Fig. 4 The expression levels of IgA, IgG, IgM in serum (n=6). (A) The expression levels of IgA; (B) The expression levels of IgG; (C) The expression levels of IgM. * $P < 0.05$, ** $P < 0.01$, *** $P < 0.001$.

3.4.4 Spleen immune status

The spleen plays a crucial role in the regulating immune responses. As described in **Section 3.4.1**, CTX significantly downregulated the spleen index. To better understand how AR and FAR improve spleen function, the tissue structure and LYMPH proliferation were examined. As shown in **Fig. 5A**, CTX significantly damaged the structure, which included a significant loss of white and red pulp. However, the spleen tissue recovered after AR and FAR intervention, while the white pulp area, rich in T and B cells, expanded. Concanavalin A (ConA) was used to assess the T cell proliferation, which was substantially lower in the CTX mice compared to the Control ($P < 0.001$) **(Fig. 5B)**. Compare with CTX group, the proliferation of spleen T lymphocytes in FAR group was significantly increased. However, there was no significant difference between AR group and CTX group. LPS was used to measure the B cell proliferation, which was considerably lower in the CTX group relative to the Control ($P < 0.001$) **(Fig. 5C)**. In comparison with the CTX mice, FAR exposure considerably elevated the proliferation rate of the B cell, while no notable differences between the CTX and AR groups.

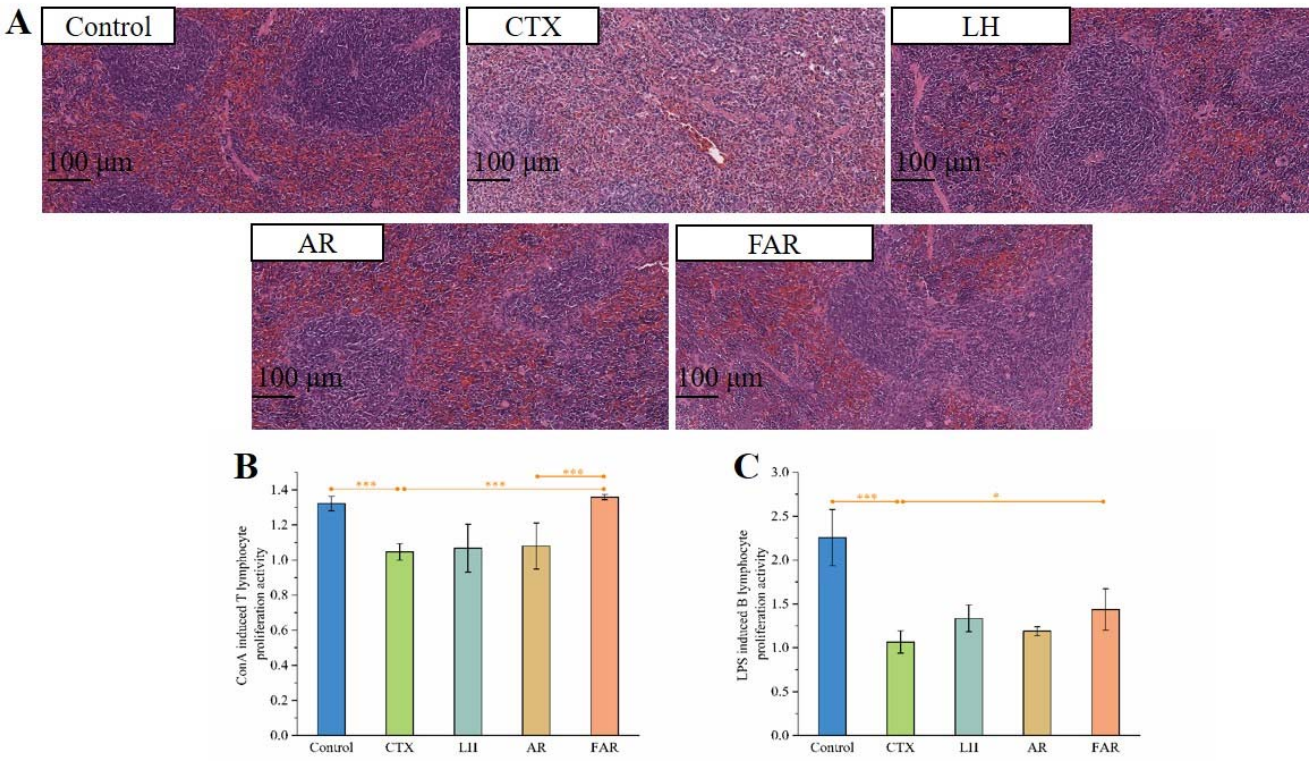


Fig. 5 Spleen immune status (A) HE analysis of spleen; (B) T lymphocyte proliferation activity induced by ConA; (C) B lymphocyte proliferation activity induced by LPS. (n=3). * $P < 0.05$, ** $P < 0.01$, *** $P < 0.001$.

3.4.5 HE and AB-PAS of the jejunum and colon

CTX not only affects spleen function but also causes intestinal mucosal damage and intestinal crypt cell apoptosis, consequently reducing intestinal villi length and crypt thickness. HE staining was employed to measure the jejunal and colonic morphological changes and evaluate the CTX damage to the different intestinal sites. As illustrated in **Fig. 6A**, the CTX group showed significant jejunal tissue damage compared with the Control group. This included reduced villus length and crypt depth, partial mucosal and submucosal layer separation, and severe intestinal tissue damage. After treatment, the LH, AR, and FAR groups displayed

similar intestinal tissue morphology to the Control group, with neatly arranged, tightly packed villi. As shown in **Fig. 6C-D**, semiquantitative analysis showed that AR significantly extended the villus length ($P < 0.001$), while FAR and LH substantially increased the crypt depth ($P < 0.001$). The CTX group showed epithelial cell damage in the colonic tissue, while the other groups maintained a relatively intact structure. Goblet cells are responsible for secreting mucus in the intestine, which is essential for maintaining the intestinal immune environment. Furthermore, the goblet cells in colonic and jejunal tissues were assessed via AB-PAS staining **(Fig. 6B)**. CTX significantly downregulated the jejunal goblet cells **(Fig. 6F)**, while the recovery was evident after AR and FAR intervention ($P < 0.01$). As shown in **Fig. 6G**, the goblet cells decreased significantly in the CTX mice, aligning with the jejunal findings, while the LH, AR, and FAR groups returned to near normal levels.

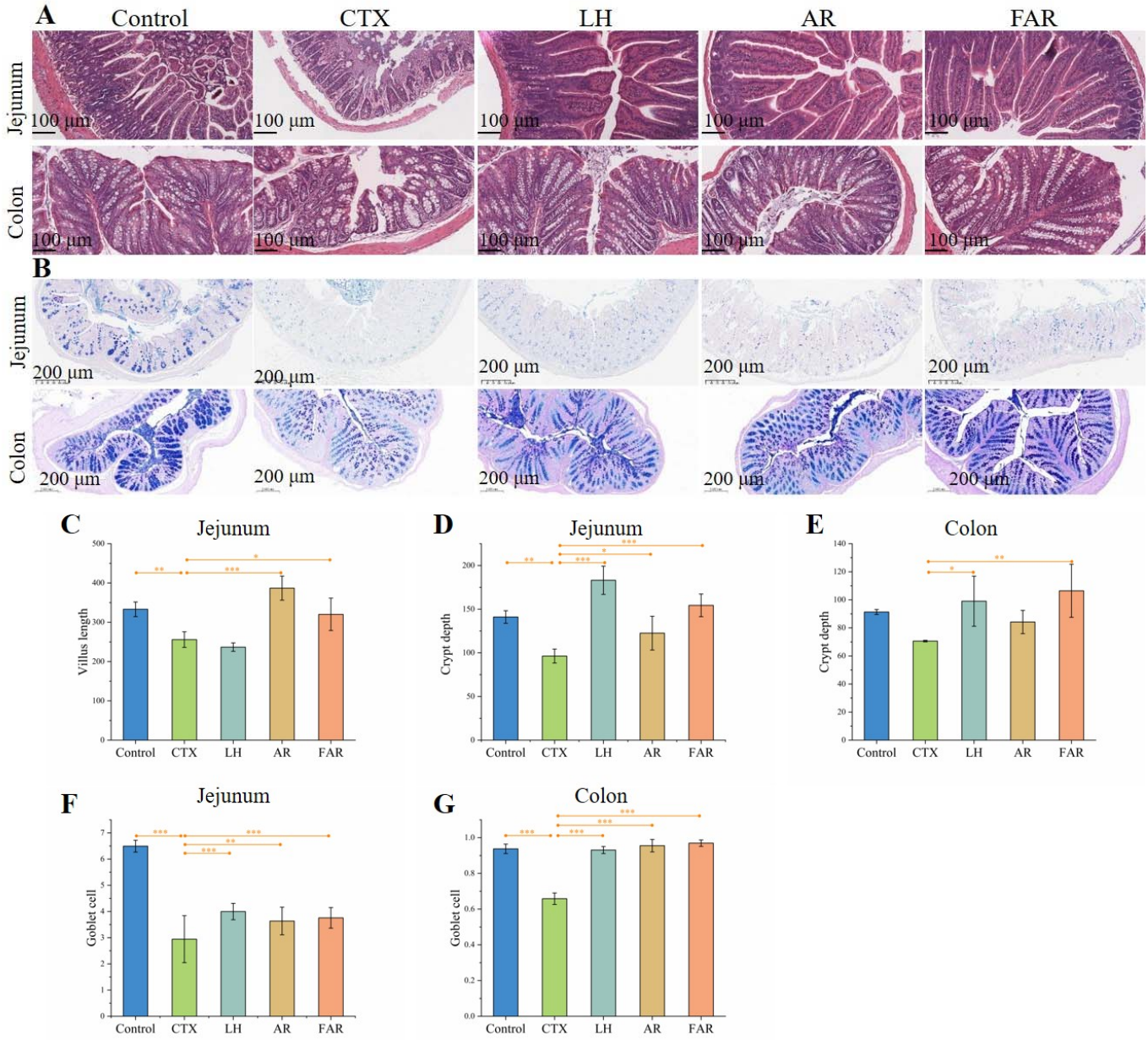


Fig. 6 HE staining and AB-PAS staining of jejunum and colon. (A) HE analysis of jejunum and colon; (B) AB-PAS analysis of jejunum and colon; (C) Villus length of jejunum; (D) Crypt depth of jejunum; (E) Crypt depth in the colon; (F) Goblet cell of jejunum; (G) Goblet cell of colon. (n=3). * $P < 0.05$, ** $P < 0.01$, *** $P < 0.001$.

3.4.6 CD4+ and CD8+ T cells in the intestinal

The balance between the number and proportion of CD8+ and CD4+ T cells is crucial for intestinal immune health, and disruptions may lead to infections, inflammation, or tumor. CTX can damage immune cells, leading to intestinal immune dysfunction. Immunohistochemical analysis showed significant CD4+ and CD8+ T cells downregulation in the colonic and jejunal tissues of the CTX mice ($P < 0.001$) (Fig. 7), In the jejunum, AR increased the expression level of CD4+ T cells ($P < 0.001$) but did not enhance CD8+ T cell expression, while FAR promoted the co-expression of both CD4+ and CD8+ T cells while maintaining the CD4+/CD8+ ratio, the CD4+/CD8+ ratios of jejunum in the Control, CTX, LH, AR, and FAR groups were 0.78± 0.05%, 0.73 ± 0.13%, 0.39 ± 0.18%, 1.69 ± 0.29%, and 0.79 ± 0.09%, respectively, these results are generally consistent with studies by Jia et al. and Xie et al[27, 31]. In the colon, both AR and FAR significantly reversed the CTX-induced downregulation of T cells and preserved the CD4+/CD8+ ratio, with FAR demonstrating a more pronounced effect, the CD4+/CD8+ ratios in the Control, CTX, LH, AR, and FAR groups were 3.63 ± 0.18%, 5.47 ± 0.08%, 9.89 ± 1.97%, 5.55 ± 2.23%, and 4.11 ± 1.48%, respectively, aligning with the findings of Deng et al[32].

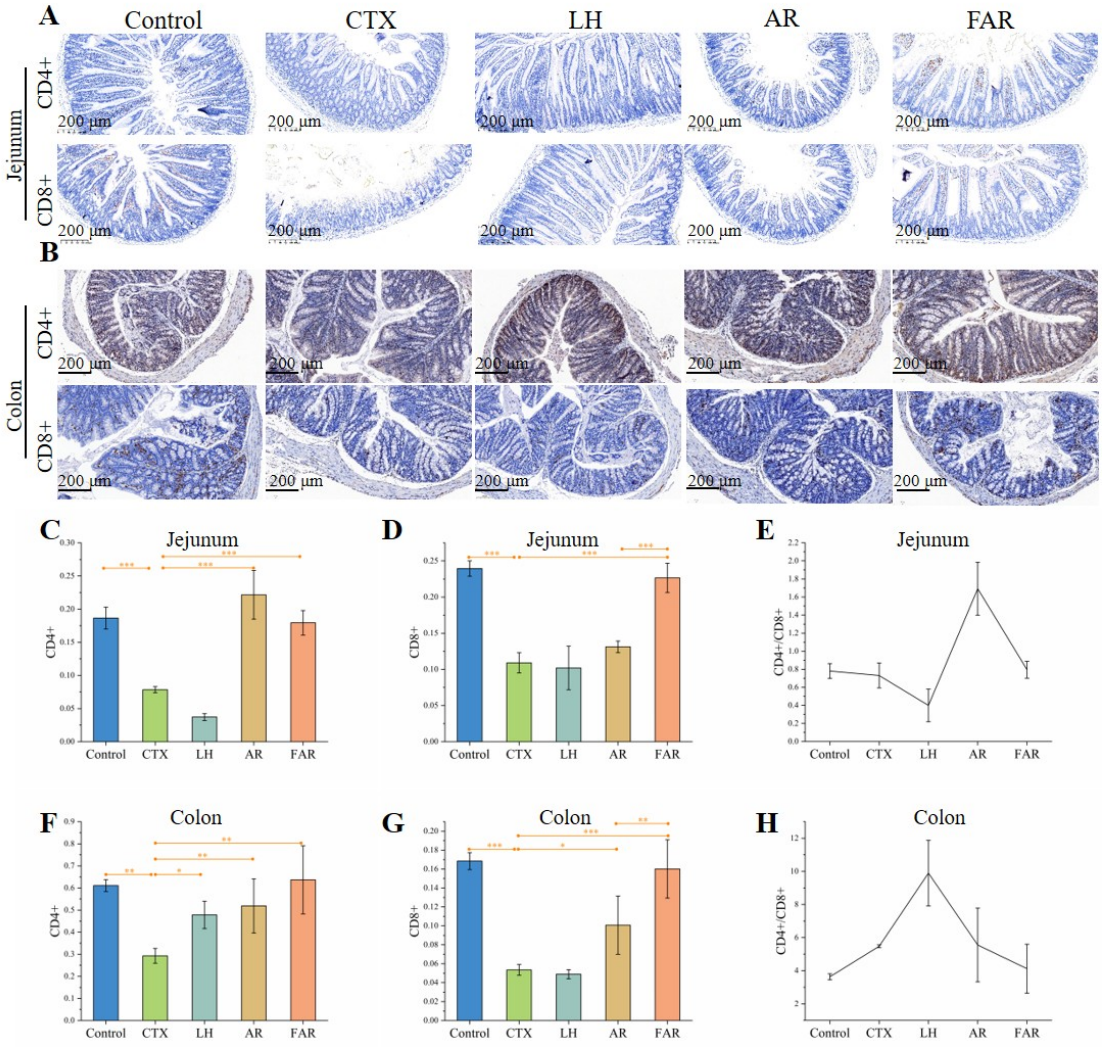


Fig. 7 Immunohistochemistry of CD4+ and CD8+ T cells. (A) CD4+ and CD8+ T cells expression of jejunum; (B) CD4+ and CD8+ T cells expression of colon; (C-E) Using Image J software to analyze the number and ratio of CD4+ and CD8 T+ cells positivity in the jejunum; (F-H) CD4+ and CD8+ T cells positivity rates and their ratio in the colon. (n=3). * $P < 0.05$, ** $P < 0.01$, *** $P < 0.001$.

3.4.7 The intestinal ZO-1, occludin, and claudin-1 levels - immunohistochemistry

CTX can seriously damage the intestinal mucosal barrier, leading to immune system disorders. Therefore, this study assessed three key proteins in intestinal tight junctions: claudin-1, occludin, and ZO-1. (**Fig. 8A-B**). In the jejunum (**Fig. 8C-E**), CTX administration significantly downregulated the expression of occludin and claudin-1 ($P < 0.05$). Following intervention with AR, FAR, and LH, the expression of ZO-1 and occludin was significantly upregulated ($P < 0.05$), while claudin-1 also exhibited an upward trend. In the colon (**Fig. 8F-H**), the expression of occludin and claudin-1 was significantly downregulated in the CTX group. Both AR and FAR interventions significantly upregulated their expression ($P < 0.05$), and returned to the same level as the control group. Although ZO-1 showed an increasing trend, the difference compared to the CTX group was not statistically significant.

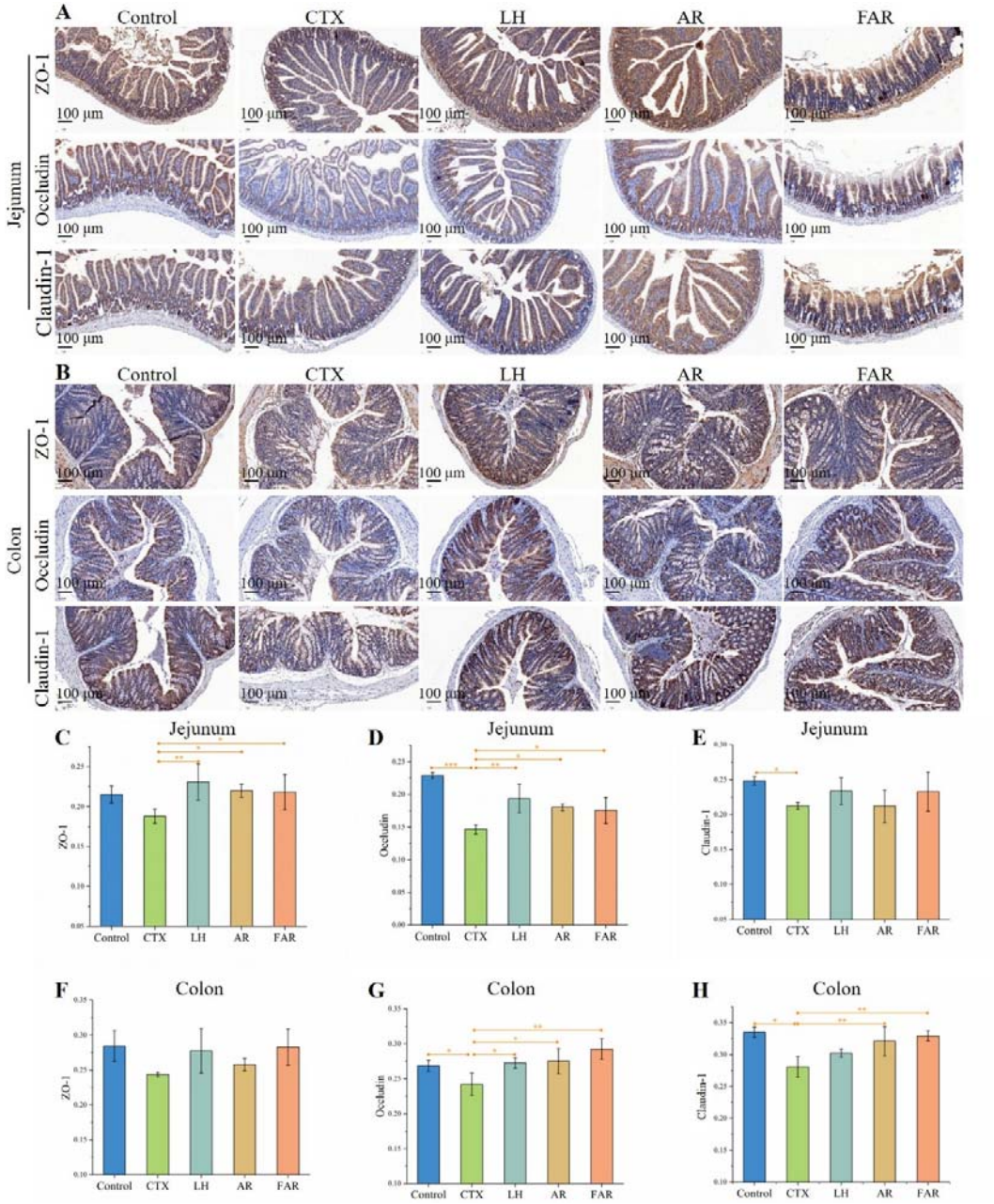


Fig. 8 Immunohistochemistry was used to measure the expression of ZO-1, occludin, and claudin-1. (A) Jejunal image; (B) Colonic image; (C-E) Quantitative analysis of ZO-1, occludin, and claudin-1 in the jejunum; (F-H) Quantitative analysis of ZO-1, occludin, and claudin-1 in the colon. (n=3). * $P < 0.05$, ** $P < 0.01$, *** $P < 0.001$.

3.4.8 The protein expression of ZO-1, occludin, claudin-1, p-P65 and p-IκBα

Fig. 9A&B shows the Western blotting results. Although CTX significantly downregulated the occludin and claudin-1 proteins ($P < 0.001$, compared to Control group), AR and FAR reversed this effect ($P < 0.05$), with FAR outperforming AR. In the jejunum, FAR increased the expression levels of ZO-1, occludin and claudin-1 by 123.28%, 119.05% and 261.71%, respectively, compared to CTX; while AR increased them by 67.67%, 95.25% and 133.81%, respectively, compared to CTX (**Fig. 9C-E**). In the colon, FAR increased the expression levels of ZO-1, occludin and claudin-1 by 88.14%, 100.72% and 179.29%, respectively, compared to the CTX; while AR increased them by 59.14%, 141.67% and 64.41%, respectively, compared to CTX (**Fig. 9H-J**). And FAR was more effective than AR. This is consistent with the results of immunohistochemistry (**section 3.4.7**). The phosphorylation levels of P65 and IκBα are key indicators of NF-κB pathway activation, and excessive activation of NF-κB typically contributes to various inflammatory conditions. As shown in **Fig. 9F&G**, the relative protein expression of p-P65/P65 and p-IκBα/IκBα in the jejunum was significantly upregulated by CTX ($P < 0.001$), while both AR and FAR interventions restored their levels close to normal. Similar results were observed in the colon (**Figs. 9L&N**), and Zhu et al.'s research also reached the same conclusion[21], where AR and FAR significantly downregulated p-P65 and p-IκBα ($P < 0.001$). Therefore, AR and FAR can inhibit the p-P65 and p-IκBα expression by controlling the NF-κB pathway, suppressed inflammation, and restored intestinal immune balance, showing consistency in both the jejunum and colon.

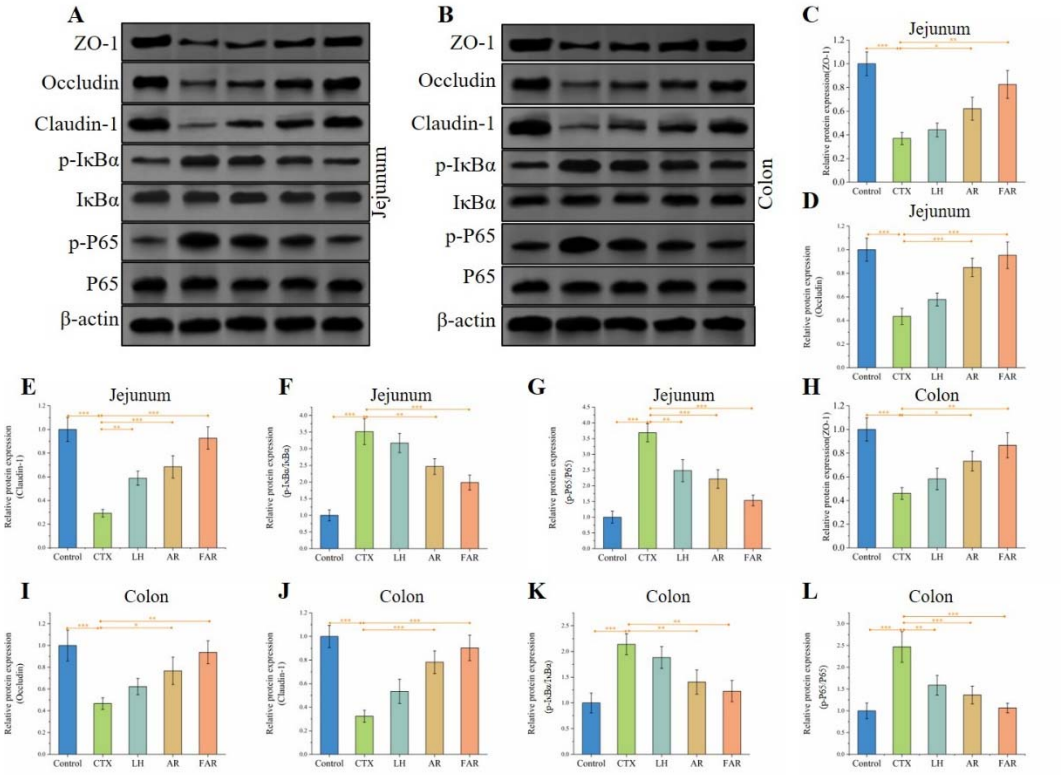


Fig. 9 The recovery effect and immune regulatory mechanism of AR and FAR on CTX induced intestinal barrier injury in mice. (A-B) Phosphorylation level of p65 and IκBα in total protein extracts from jejunum and colon, and occluding and claudin-1 protein expression, measured by Western blot. (C-G) The relative expression proteins levels of ZO-1, occludin, claudin-1, p-P65, and p-IκBα in the jejunum were analyzed (H-L) The relative expression proteins levels of ZO-1, occludin, claudin-1, p-P65, and p-IκBα in the jejunum. Image. J software was used to determine the grayscale values. (n=3). * $P < 0.05$, ** $P < 0.01$, *** $P < 0.001$.

3.4.9 Gut microbiota analysis

16S rRNA sequencing was utilized to analyze the impact of AR and FAR on the microbiota in the intestines of the immunosuppressed mice. The Sob, Chao, and ACE indexes denote the richness of the microbial community. These indices were higher in the administration groups (AR and FAR groups) than in the CTX group, indicating that AR and FAR increased the richness of the intestinal flora **(Figs. 10A-C)**. Furthermore, the structural similarities between the microbial communities were examined via beta-diversity analysis **(Fig. 10D)**. The PCA results showed significant clustering and separation between the groups, with significant changes in the intestinal microbiota of the mice in the Control and CTX groups, while the AR and FAR groups shifted towards the Control group. However, no changes were evident after LH treatment, suggesting that it might not affect CTX-induced immunodeficiency by modulating the microbiota.

The taxonomic characteristics of the groups were assessed to determine the specific alterations in the gut microbes. The abundant phyla primarily included Firmicutes and Bacteroidetes **(Fig. 10E)**. Treatment with CTX increased the Pseudomonadota (formerly Proteobacteria) abundance, AR and FAR exposure reversed these changes **(Fig. 10F)**. AR and FAR treatment altered the relative abundance of various bacterial genera **(Fig. 10G)**. As depicted in **Fig. 10H-P**, compared with the CTX mice, the abundance of g__*Ligilactobacillus*, g__unclassified_f__*Lachnospiraceae*, g__*Lachnospiraceae*_NK4A136_group, g__A2, g__*Blautia* (f__*Lachnospiraceae*), g__*Muribaculum*, and g__norank_f__*Oscillospiraceae* increased in both the AR and FAR groups, while the g__*Faecalimonas* level was higher in the AR group. LEfSe analysis was performed to identify the primary gut microbiota in each group **(Fig. 10O)**. The LDA histogram indicated that the CTX group primarily showed p__Pseudomonadota and c__Gammaproteobacteria clustering. The AR group was enriched with c__Clostridia, g__norank_f__*Oscillospiraceae,* and g__A2, while the dominant bacteria in the FAR group were o__Lachnospirales, f__*Lachnospiraceae*, g__unclassified_f__*Lachnospiraceae*, g__*Blautia*, and g__*Muribaculum.*

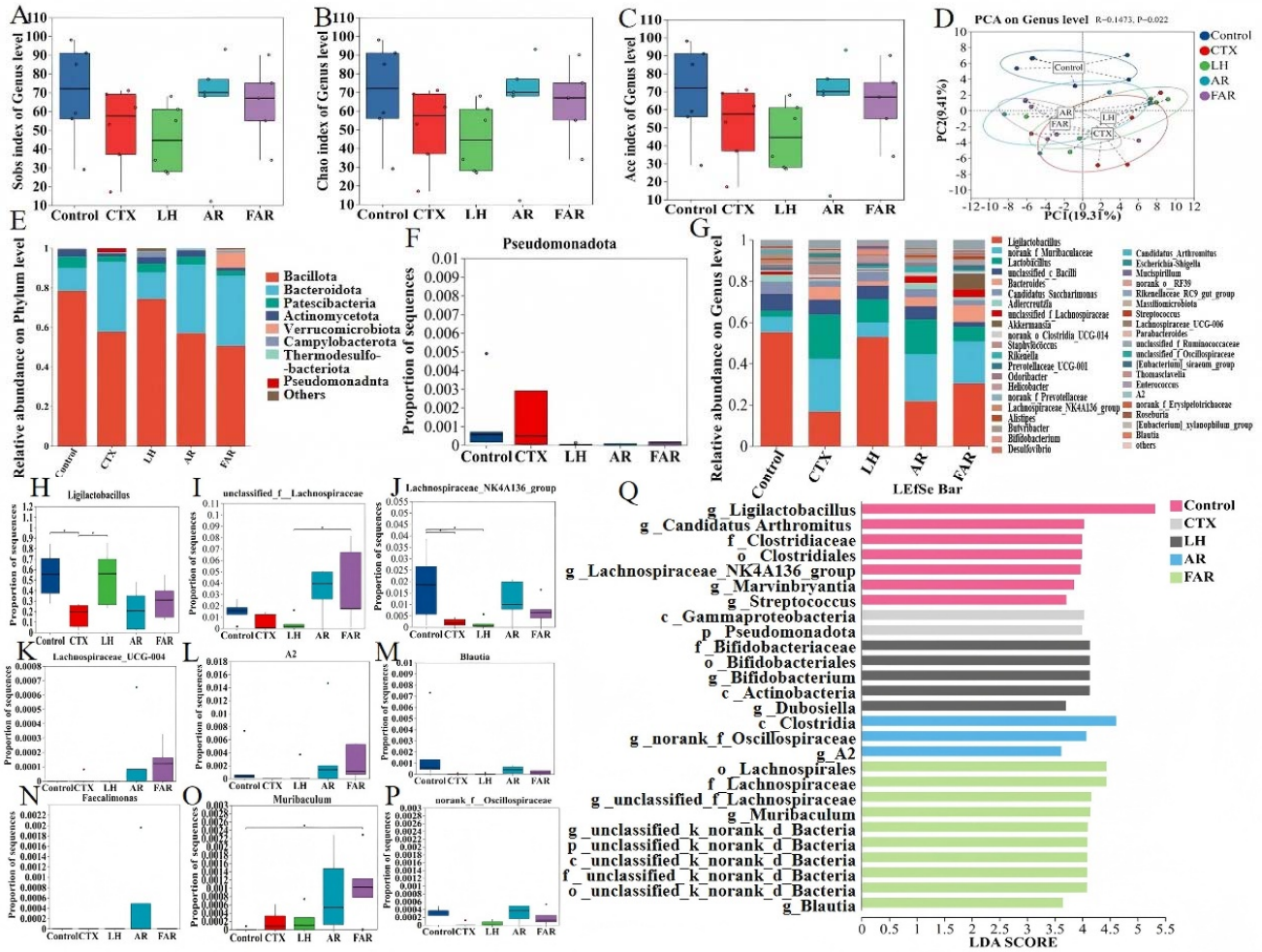


Fig. 10 The gut microbiota was analyzed in feces by 16S rRNA sequencing (n = 5 or 6). Estimation of the microbial community with the Sob index (A), Chao index (B), and Ace index (C) at the genus level. Statistical analysis by Kruskal Wallis H test with Games-Howell post hoc test. (D) The Genus-level Principal Component analysis (PCA) illustrated the β diversity of the gut microbiota. (E) Relative abundance of the gut microbiota. Phylum level taxonomy is presented as a percentage of total sequences. (F) Phylum abundance of Pseudomonadota. (G) The relative abundance of bacteria with intergroup differences at the genus level. Statistical analysis by Kruskal-Wallis H test with Dunn's post hoc test. (H-P) Genus abundance of Ligilactobacillus, unclassified_f__Lachnospiraceae, Lachnospiraceae_NK4A136_group, Lachnospiraceae_UCG-004, A2, Blautia, Faecalimonas, Muribaculum, and g__norank_f__Oscillospiraceae. Data are expressed as mean ± SD (n = 5 or 6). (Q) Linear discriminant analysis (LDA) column chart showing the analysis from the phylum to the genus levels. * $P < 0.05$, ** $P < 0.01$.

4. Discussion

To develop a functional probiotic beverage with a pleasant mouthfeel, we adopted a "extract-then-ferment" strategy. This approach is superior to direct fermentation of the crude herbal material because it ensures a homogeneous liquid matrix, which is crucial for avoiding an unpleasant coarse texture and for enabling industrial scalability[33, 34]. In the liquid culture system, LGG was in full contact with water-soluble substrates, which created favorable conditions for subsequent enzymatic bioconversion. Our preliminary optimization also showed that a fermentation temperature of 30°C could better balance bacterial growth and metabolite preservation, which is consistent with the results reported by Wang et al.[35]. In summary, these process parameters lay the material foundation for the alteration of sensory and functional properties of fermented products.

The increased sweetness and saltiness detected by the electronic tongue can be mechanistically attributed to specific enzymatic pathways driven by LGG. LGG can secrete glycoside hydrolases and peptidases[36], which degrade long-chain *Astragalus Radix* polysaccharides into short-chain oligosaccharides or monosaccharides, and cleave sugar moieties from flavonoid glycosides, thereby increasing the concentration of perceptible sweet-tasting components. Meanwhile, it promotes protein breakdown in AR, releasing free amino acids, including "sweet" amino acids (e.g., alanine). Zhang et al.[37] also reported that probiotic fermentation of goji juice significantly increased glucose and sweetness-contributing amino acids, effectively masking bitterness and enhancing overall sweetness perception. During fermentation, the accumulation of organic acids decreases the pH and promotes the dissolution of mineral ions in the plant matrix[38], which may enhance the response of saltiness-sensitive sensors. At the same time, the action of these enzymatic also changes the volatile profile spectrum by the e-nose. For example, dehydrogenases from *Lactobacillus* reduce "bean-like" aldehydes such as hexanal, to the corresponding alcohol, thereby reducing odors[39]. Similarly, Sun et al.[40] observed that fermentation of mung bean milk by lactic acid bacteria effectively metabolized hexanal to alcohols, successfully eliminating bean flavor and promoting the formation of esters.

In order to explore the compositional changes of AR during LGG fermentation, a combination of chemical analysis and untargeted metabolomics was used. The results showed that LGG fermentation significantly increased the content of flavonoids in AR, which was consistent with the report of Tu et al[41]. The increase in flavonoids may be related to bioconversion processes (e.g., transglucoside, demethylation, esterification, and hydrogenation) that promote the release of glycosidic and conjugated flavonoids. KEGG pathway analysis further confirmed that the expression of biosynthetic pathways related to flavonoid synthesis (including flavonoid, flavonol and other biosynthetic pathways) was up-regulated, which was consistent with the experimental phenomenon that the total flavonoid content increased by 23.5%. In line with these findings, Merenkova et al. pointed out that fermentation can improve the yield of isoflavone aglycone in cereals[42]; Gaya et al. demonstrated that lactic acid bacteria can convert bound isoflavones into free forms with biological activity through deglycosylation and demethylation[43]. After LGG fermentation, the content of polysaccharide decreased, which may be related to the metabolic utilization of polysaccharide by LGG. *Astragalus Radix* polysaccharides mainly consists of glucose and galactose[44]. LGG can secrete a variety of glycoside hydrolases (such as β-glucosidase/β-galactosidase) to degrade the molecular weight of polysaccharide. Previous studies have shown that changes in the molecular weight of polysaccharides can help improve their biological activity and intestinal absorption efficiency[45]. Pei et al. reported that *Lactobacillus rhamnosus* 6224 could reduce the molecular weight of Lonicerae polysaccharide and enhance its antioxidant activity[46], which was consistent with our study. Metabolomics analysis also showed that the linoleic acid metabolic pathway was up-regulated after fermentation, and this pathway contributed significantly to the formation of the unique flavor of FAR[47]. Concurrently, the biosynthetic pathways of phenylalanine, tyrosine and tryptophan are down-regulated, which helps to reduce the bitter taste of fermented beverages[48]. The changes in the synthesis pathways of pantothenic acid and coenzyme A affect the functional composition

and aroma composition of the product[49]. Studies have also found that specific amino acids such as alanine increase, and this change can not only neutralize salty and bitter tastes, but also enhance overall sweet perception[50]. The fermentation process does not only change the content of a single component, but also reshapes the chemical composition of AR as a whole to form a new matrix with better bioactivity and bioavailability.

Fermentation induces material transformations in AR. These transformations determine its resultant biological effects. The main activity of AR is immunomodulation, so we used a CTX-induced immunosuppressed mouse model to study the effects of fermentation on bioactivities. In this study, Both AR and FAR increased the immune organ indices of the Balb/c mice, and the FAR group showing better effects. CTX also lead to strong bone marrow suppression and blood cell deficiency. The AR, FAR, and LH groups showed elevated WBC, LYMPH, and PLT counts, reversing the CTX-induced defects in blood cell indexes. Wang et al. found that fermentation treatment significantly enhanced the efficacy of loofah in alleviating CTX-induced immunosuppression. It increased the thymus index and the counts of WBC, which is content with our results[51].

Immunoglobulins play a crucial role in the humoral immune response. Our research measured three main types of antibodies: IgA, IgM, and IgG. Compared to the CTX group, both AR and FAR increased the expression levels of IgA, IgM, and IgG. FAR intervention also significantly improved the expression level of IgM compared to the AR group, and this indicates that FAR has a more significant impact on the initial immune response[52]. Similarly, Li et al. demonstrated that *Astragalus Radix* polysaccharides significantly increase the levels of IgA, IgM, and IgG in immunosuppressed mice induced by CTX[53].

Previous research has proved the spleen-enhancing effects of AR extract[54, 55]. This study examined the immune status of the spleen, the FAR group displayed B and T cells proliferation in the spleen compare to CTX group. Chen et al. also found that probiotic fermentation of AR can improve the spleen index in immunosuppressive mice, and promote the expression of T and B cells in spleen[56]. In the HE staining results, the CTX group exhibited damage to white pulp of the spleen. The white pulp contained critical structures for T and B cells, such as the periarterial lymphoid sheath and lymphoid follicles. Both AR and FAR have capabilities in promoting the recovery of white pulp tissue, this corresponds to the results of B and T cells proliferation.

The gut is an important immune organ. The appropriate quantity and balance of CD4+ T and CD8+ T cells are essential for managing intestinal inflammatory responses and maintaining immune tolerance[57]. Wang et. al found that *Atractylodes lancea Rhizome* polysaccharide can enhance the intestinal mucosal immunity by improving the expression of CD4+ T and CD8+ T lymphocytes[26]. Our results showed that CTX inhibited the levels of expression of CD4+ T and CD8+ T cells. However, these effects were significantly reversed after treatment with AR and FAR, and FAR also maintain the ratio of CD4+/CD8+ T cells.

The intestinal immune system is a complex and dynamically balanced system. It consists of physical barriers, chemical defenses, innate immunity and adaptive immunity. Moreover, it relies on the coordinated

regulation of the intestinal microbiota[58]. The intestinal barrier plays an important role in immunity. Tight junctions, the primary structural elements of this barrier, are formed with key proteins, including ZO-1, clauding-1, and occludin[59]. Goblet cells are glands that produce mucin. Mucin forms a mucus layer, which can separate the materials in cavities from the intestinal epithelium and prevent the invasion of pathogenic microorganisms[60]. CTX induces intestinal damage through multiple mechanisms. It disrupts mucosal integrity by impairing goblet cells and downregulating tight junction protein expression. And it also reduces LYMPH counts and causes dysbiosis of the intestinal microbiota. This study explored the impact of AR and FAR on intestinal mucosal injury. CTX significantly down regulated the expression of ZO-1, occludin and claudin-1 proteins, while FAR reversed this trend and the effect was better than AR. Li et al. also obtained similar results, after taking fermented Ganoderma lucidum and Semen Raphani, the expression levels of ZO-1, occludin, and claudin-1 in mice were upregulated, thereby repairing the intestinal barrier damage caused by CTX[61].

The immunomodulatory effects of AR and FAR are associated with the NF-κB pathway. In the CTX group, p-P65 and p-IκBα were upregulated, indicating inflammation and resulting in intestinal immune dysfunction. After receiving FAR intervention, they returned to levels close to the control group. This may be attributed to the effects of flavonoids, flavonoids can exert anti-inflammatory activity by inhibiting the NF-κB pathway, which can explain the downregulation of p-P65 and p-IκBα in FAR[62].

The active ingredients, particularly polysaccharides and flavonoids, in fermented plant products can act as prebiotics and effectively regulate intestinal microbial communities[63]. Both AR and FAR could partially reverse the imbalance of flora induced by CTX, partially restore the richness indexes (Sob, Chao and ACE), and promote the community structure (PCA) to the control group. Notably, both significantly reduced the relative abundance of the phylum Pseudomonas which is often associated with intestinal inflammation and epithelial damage. Wang et al.[13] also found that AR fermentation by *Bacillus subtilis* could effectively reshape the intestinal flora composition of disease model animals by inhibiting harmful Pseudomonas. The genus level analysis showed that after the intervention of FAR, the bacteria producing SCFAs were specifically enriched, including unclassified *Lachnospirillaceae*, *Blautia* and *Muribaculum*. These bacterial genera play a key role in maintaining intestinal homeostasis. *Lachnospirillaceae* are major producers of butyrate, which can effectively enhance the integrity of the intestinal epithelial barrier[64]. *Blautia* produce acetic acid in large quantities, and this metabolite is essential for regulating immune homeostasis[65]. Propionic acid produced by *Muribaculum* helps to inhibit the colonization of pathogens in the gut[66]. This specific bacterial enrichment was most likely due to the degradation of long-chain polysaccharides into low molecular weight oligosaccharides during LGG fermentation. Cai et al.[67] showed that low molecular weight *Astragalus Radix* polysaccharides had better prebiotic activity and were more easily used by *Lachnospiraceae* compared with unprocessed polysaccharides. Free flavonoid aglycones released during fermentation may exert a selective prebiotic effect. Etxeberria et al. and Yan et al observed that biotransformed flavonoids can interact bidirectionally with the gut microbiota in a bidirectional manner, promoting the proliferation of *Blautia*[68]

and *Lachnospiraceae*[69], while also inhibiting the growth of pathogenic taxa. Therefore, FAR can restore CTX-induced intestinal flora imbalance by not only providing prebiotic substrates, but also producing active ingredients that are conducive to the proliferation of SCFAs producing bacteria, thereby strengthening intestinal barrier and immune function.

5. Conclusion

Here, we investigated the effects of LGG fermentation on the chemical composition, sensory profile, immunomodulatory activity, and intestinal barrier function of AR. After fermentation, the flavonoid content increased by 23.5%, which was mediated by LGG through biosynthetic pathways such as flavonoid and isoflavonoid synthesis. LGG fermentation also promoted the consumption of polysaccharides, possibly accompanied by structural modification of polysaccharides, likely due to the hydrolytic action of glycosidases. These fermentation-driven changes in the material basis influenced its sensory and biological effects. In a CTX-induced immunosuppressed mouse model, FAR demonstrated superior immunomodulatory activity. It not only restored the structure of immune organs (thymus, spleen) and the levels of blood cells, but also maintained the balance in the quantity and ratio of intestinal CD4+ T / CD8+ T cells. FAR repaired CTX-induced intestinal barrier damage by upregulating tight junction proteins such as ZO-1, occludin, and claudin-1. The increased flavonoid content positively contributed to anti-inflammatory activity, as FAR significantly inhibited the NF-κB pathway, downregulated the expression levels of p-P65 and p-IκBα proteins, and alleviated intestinal inflammation. Furthermore, FAR altered the composition of the gut microbiota by increasing microbial richness and enriching beneficial bacteria, including unclassified *Lachnospiraceae*, *Blautia* and *Muribacurella*. These experimental results and methodologies provide a novel approach to the probiotic fermentation of AR. To further develop FAR as a functional beverage, additional research on its intestinal digestion and absorption characteristics is warranted. Moreover, investigating how LGG degrades and structurally modifies polysaccharides to enhance their bioactivity represents another valuable research direction.

Ethics statement

All Institutional and National Guidelines for the care and use of animals were followed.

Conflict of interest

The authors declare that there are no conflicts of interest.

Acknowledgements

This work was financially supported by Natural Science Foundation of Jilin Province (No. YDZJ202401028ZYTS), the CAMS Innovation Fund for Medical Science (CIFMS, No. 2022-I2M-1-018), and the abilitly establishment of sustainable use for valuable chinese medicine resources (No. 2060302-2305-04).

References

[1] C. Venter, S. Eyerich, T. Sarin, et al., Nutrition and the Immune System: A Complicated Tango, Nutrients. 12 (2020) https://doi.org/10.3390/nu12030818.

[2] J.T. Campillo, C. Eiden, M. Boussinesq, et al., Adverse reactions with levamisole vary according to its indications and misuse: A systematic pharmacovigilance study, Br J Clin Pharmacol. 88 (2022) 1094-1106. https://doi.org/10.1111/bcp.15037.

[3] D. Peng, H.Y. Xing, C. Li, et al., The clinical efficacy and adverse effects of Entecavir plus Thymosin alpha-1 combination therapy versus Entecavir Monotherapy in HBV-related cirrhosis: a systematic review and meta-analysis, BMC Gastroenterol. 20 (2020) 348. https://doi.org/10.1186/s12876-020-01477-8.

[4] J. Fu, Z. Wang, L. Huang, et al., Review of the botanical characteristics, phytochemistry, and pharmacology of Astragalus membranaceus (Huangqi), Phytother Res. 28 (2014) 1275-1283. https://doi.org/10.1002/ptr.5188.

[5] Z. Guo, Y. Lou, M. Kong, et al., A Systematic Review of Phytochemistry, Pharmacology and Pharmacokinetics on Astragali Radix: Implications for Astragali Radix as a Personalized Medicine, Int J Mol Sci. 20 (2019) https://doi.org/10.3390/ijms20061463.

[6] J.L. Cao, L.Y. Liang, Y.H. Liu, et al., [Medication rules of Astragali Radix in ancient Chinese medical books based on "disease-medicine-dose" pattern], Zhongguo Zhong Yao Za Zhi. 50 (2025) 798-811. https://doi.org/10.19540/j.cnki.cjcmm.20241114.501.

[7] X. Rong, Q. Shu, Enhancing immunomodulation in cyclophosphamide-induced immunosuppressed mice through targeted modulation of butyrate-producing gut microbiota via oral administration of astragalus polysaccharides, Food Sci Nutr. 12 (2024) 7683-7695. https://doi.org/10.1002/fsn3.4386.

[8] J. Hou, A. Li, G. Wang, et al., Metabolomics analysis of Astragali Radix in Shanxi Province: Investigating the impact of various cultivation methods and growth years on metabolite profiles, Food Chem. 468 (2025) 142492. https://doi.org/10.1016/j.foodchem.2024.142492.

[9] H.J. Kwon, J. Hwang, S.K. Lee, et al., Astragaloside content in the periderm, cortex, and xylem of Astragalus membranaceus root, J Nat Med. 67 (2013) 850-855. https://doi.org/10.1007/s11418-013-0741-8.

[10] X. Zhang, Q. Miao, C. Pan, et al., Research advances in probiotic fermentation of Chinese herbal medicines, Imeta. 2 (2023) e93. https://doi.org/10.1002/imt2.93.

[11] A.R. Harper, R.C.J. Dobson, V.K. Morris, et al., Fermentation of plant-based dairy alternatives by lactic acid bacteria, Microb Biotechnol. 15 (2022) 1404-1421. https://doi.org/10.1111/1751-7915.14008.

[12] Y. Wang, X. Mei, Z. Liu, et al., Chemical Constituent Profiling of Paecilomyces cicadae Liquid Fermentation for Astragli Radix, Molecules. 24 (2019) https://doi.org/10.3390/molecules24162948.

[13] R. Wang, F. Lin, C. Ye, et al., Multi-omics analysis reveals therapeutic effects of Bacillus subtilis-fermented Astragalus membranaceus in hyperuricemia via modulation of gut microbiota, Food Chem. 399 (2023) 133993. https://doi.org/10.1016/j.foodchem.2022.133993.

[14] Y.E. Cheong, J. Kim, Y.S. Jin, et al., Elucidation of the fucose metabolism of probiotic Lactobacillus rhamnosus GG by metabolomic and flux balance analyses, J Biotechnol. 360 (2022) 110-116. https://doi.org/10.1016/j.jbiotec.2022.11.002.

[15] R. Suissa, T. Olender, S. Malitsky, et al., Metabolic inputs in the probiotic bacterium Lacticaseibacillus rhamnosus contribute to cell-wall remodeling and increased fitness, NPJ Biofilms Microbiomes. 9 (2023) 71. https://doi.org/10.1038/s41522-023-00431-2.

[16] J. He, L. Chen, B. Chu, et al., Determination of Total Polysaccharides and Total Flavonoids in Chrysanthemum morifolium Using Near-Infrared Hyperspectral Imaging and Multivariate Analysis, Molecules. 23 (2018) https://doi.org/10.3390/molecules23092395.

[17] Z. Nizioł-Łukaszewska, D. Furman-Toczek, M. Zagórska-Dziok, Antioxidant activity and cytotoxicity of Jerusalem artichoke tubers and leaves extract on HaCaT and BJ fibroblast cells, Lipids Health Dis. 17 (2018) 280. https://doi.org/10.1186/s12944-018-0929-8.

[18] H. Kim, S. Humanyun, T. Kim, et al., Enhancement of bioactive compounds, antioxidant capacity, and inhibitory effects on mushroom tyrosinase, α-glucosidase, and nitric oxide production in sorghum (Sorghum bicolor L.) via solid-state fermentation with Monascus purpureus, Food Sci Biotechnol. 34 (2025) 181-192. https://doi.org/10.1007/s10068-024-01642-9.

[19] W. Yao, S. Ma, H. Wu, et al., Flavor profile analysis of grilled lamb seasoned with classic salt, chili pepper, and cumin (Cuminum cyminum) through HS-SPME-GC-MS, HS-GC-IMS, E-nose techniques, and sensory evaluation on Sonit sheep, Food Chem. 454 (2024) 139514. https://doi.org/10.1016/j.foodchem.2024.139514.

[20] C. Han, C. Shi, L. Liu, et al., Majorbio Cloud 2024: Update single-cell and multiomics workflows, Imeta. 3 (2024) e217. https://doi.org/10.1002/imt2.217.

[21] Z. Zhu, Y. Luo, L. Lin, et al., Modulating Effects of Turmeric Polysaccharides on Immune Response and Gut Microbiota in Cyclophosphamide-Treated Mice, J Agric Food Chem. 72 (2024) 3469-3482. https://doi.org/10.1021/acs.jafc.3c05590.

[22] L. Yu, X. Shi, X. Lu, et al., Rehmannia glutinosa polysaccharides alleviate cyclophosphamide-induced immunosuppression by enhancing immunity and restoring intestinal homeostasis, Int J Biol Macromol. 311 (2025) 143692. https://doi.org/10.1016/j.ijbiomac.2025.143692.

[23] A. Xie, F. He, L. Wang, et al., Phellinus igniarius alcohol extract restores the immune homeostasis in cyclophosphamide induced immunocompromised mice, Journal of Functional Foods. 129 (2025) 106861. https://doi.org/https://doi.org/10.1016/j.jff.2025.106861.

[24] Z.Q. Dai, L.J. Shang, Y.S. Wei, et al., Immunomodulatory Effects of Microcin C7 in Cyclophosphamide-Induced Immunosuppressed Mice, J Agric Food Chem. 71 (2023) 12700-12714. https://doi.org/10.1021/acs.jafc.3c01033.

[25] Y. Zhang, W. Ji, H. Qin, et al., Astragalus polysaccharides alleviate DSS-induced ulcerative colitis in mice by restoring SCFA production and regulating Th17/Treg cell homeostasis in a microbiota-dependent manner, Carbohydr Polym. 349 (2025) 122829. https://doi.org/10.1016/j.carbpol.2024.122829.

[26] D. Wang, Y. Dong, Y. Xie, et al., Atractylodes lancea Rhizome Polysaccharide Alleviates Immunosuppression and Intestinal Mucosal Injury in Mice Treated with Cyclophosphamide, J Agric Food Chem. (2023) https://doi.org/10.1021/acs.jafc.3c05173.

[27] J. Jia, Y. Gu, C. Yan, et al., Oyster polysaccharides alleviate cyclophosphamide-induced immunosuppression in mice by modulating lymphocytes profile and maintaining intestinal homeostasis, Int J Biol Macromol. 319 (2025) 145273. https://doi.org/10.1016/j.ijbiomac.2025.145273.

[28] E. Bolyen, J.R. Rideout, M.R. Dillon, et al., Reproducible, interactive, scalable and extensible microbiome data science using QIIME 2, Nat Biotechnol. 37 (2019) 852-857. https://doi.org/10.1038/s41587-019-0209-9.

[29] Q. Wang, L. Li, L. Hu, et al., Investigation of the solid-state fermentation of Astragalus membranaceus residue with Cordyceps militaris: effects on phenolic profile and in vitro neuroprotective activity, Food Chem. 493 (2025) 145846. https://doi.org/10.1016/j.foodchem.2025.145846.

[30] C. Li, S. Duan, Y. Li, et al., Polysaccharides in natural products that repair the damage to intestinal mucosa caused by cyclophosphamide and their mechanisms: A review, Carbohydrate Polymers. 261 (2021) 117876. https://doi.org/https://doi.org/10.1016/j.carbpol.2021.117876.

[31] X. Xie, Y. Gu, Y. Liu, et al., An inulin-type fructan from Codonopsis pilosula ameliorates cyclophosphamide-induced immunosuppression and intestinal barrier injury in mice, Int J Biol Macromol. 310 (2025) 143312. https://doi.org/10.1016/j.ijbiomac.2025.143312.

[32] Y. Deng, R. Wang, X. Li, et al., Fish Oil Ameliorates Vibrio parahaemolyticus Infection in Mice by Restoring Colonic Microbiota, Metabolic Profiles, and Immune Homeostasis, J Agric Food Chem. 71 (2023) 6920-6934. https://doi.org/10.1021/acs.jafc.2c08559.

[33] Q. Zhang, S. Yan, Y. Luo, et al., Probiotics fermentation enhanced the bioactive properties of Gnaphalium affine water extract and improved regulation ability of gut microbiota, Food Chem X. 25 (2025) 102106. https://doi.org/10.1016/j.fochx.2024.102106.

[34] P. Biernacka, K. Felisiak, I. Adamska, et al., Ultrasound pre-treatment of Ginkgo biloba leaves enhances the functional and sensory properties of the fermented beverage, Food Chem. 499 (2026) 147329. https://doi.org/10.1016/j.foodchem.2025.147329.

[35] H. Wang, Y. Tao, Y. Li, et al., Application of ultrasonication at different microbial growth stages during apple juice fermentation by Lactobacillus plantarum: Investigation on the metabolic response, Ultrason Sonochem. 73 (2021) 105486. https://doi.org/10.1016/j.ultsonch.2021.105486.

[36] L. You, R. Lv, H. Jin, et al., A large-scale comparative genomics study reveals niche-driven and within-sample intra-species functional diversification in Lacticaseibacillus rhamnosus, Food Res Int. 173 (2023) 113446. https://doi.org/10.1016/j.foodres.2023.113446.

[37] J.G. Zhang, J.J. Wang, W.W. Zhang, et al., Metabolomics and HS-SPME-GC-MS-based analysis of quality succession patterns and flavor characteristics changes during the fermentation of Lycium barbarum and Polygonatum cyrtonema compound wine, Food Res Int. 184 (2024) 114270. https://doi.org/10.1016/j.foodres.2024.114270.

[38] J. Gan, X. Kong, K. Wang, et al., Effect of fermentation using different lactic acid bacteria strains on the nutrient components and mineral bioavailability of soybean yogurt alternative, Front Nutr. 10 (2023) 1198456. https://doi.org/10.3389/fnut.2023.1198456.

[39] Z. Hu, P. Jia, Y. Bai, et al., Characterisation of five alcohol dehydrogenases from Lactobacillus reuteri DSM20016, Process Biochemistry. (2019) https://doi.org/10.1016/j.procbio.2019.08.010.

[40] Z. Sun, L. Liu, R. Li, et al., Improved nutritional composition and flavor of mung bean yogurt through fermentation with Lactiplantibacillus plantarum SF28, Food Bioscience. (2025) https://doi.org/10.1016/j.fbio.2025.106338.

[41] F. Tu, C. Xie, H. Li, et al., Effect of in vitro digestion on chestnut outer-skin and inner-skin bioaccessibility: The relationship between biotransformation and antioxidant activity of polyphenols by metabolomics, Food Chem. 363 (2021) 130277. https://doi.org/10.1016/j.foodchem.2021.130277.

[42] S. Merenkova, O. Zinina, I. Potoroko, Fermented Plant Beverages Stabilized with Microemulsion: Confirmation of Probiotic Properties and Antioxidant Activity, Fermentation. (2022) https://doi.org/10.3390/fermentation8120723.

[43] P. Gaya, Á. Peirotén, M. Medina, et al., Isoflavone metabolism by a collection of lactic acid bacteria and bifidobacteria with biotechnological interest, International Journal of Food Sciences and Nutrition. (2016) https://doi.org/10.3109/09637486.2016.1144724.

[44] G. Chen, N. Jiang, J. Zheng, et al., Structural characterization and anti-inflammatory activity of polysaccharides from Astragalus membranaceus, International Journal of Biological Macromolecules. (2023) https://doi.org/10.1016/j.ijbiomac.2023.124386.

[45] Y. Cai, Z. Si, Y. Jiang, et al., Structure-activity relationship of low molecular weight Astragalus membranaceus polysaccharides produced by Bacteroides, Carbohydrate Polymers. (2023) https://doi.org/10.1016/j.carbpol.2023.121036.

[46] F. Pei, X. Cao, X. Wang, et al., Structural characteristics and bioactivities of polysaccharides from blue honeysuckle after probiotic fermentation, LWT - Food Science and Technology. (2022) https://doi.org/10.1016/j.lwt.2022.113764.

[47] Q. Ma, Y. Chai, A. Huang, Untargeted metabolomics revealed the metabolites profile and conjugated linoleic acid formation mechanisms of fermented milk produced by novel Limosilactobacillus fermentum L1, LWT - Food Science and Technology. (2025) https://doi.org/10.1016/j.lwt.2025.118686.

[48] X. Li, Y. You, B. Xue, et al., Decoding microbiota and metabolite transformation in inoculated fermented suansun using metagenomics, GC–MS, non-targeted metabolomics, and metatranscriptomics:Impacts of different Lactobacillus plantarum strains, Food Research International. (2025) https://doi.org/10.1016/j.foodres.2025.115847.

[49] Z. Tian, L. Liu, L. Wu, et al., Enhancement of vitamin B6 production driven by omics analysis combined with fermentation optimization, Microbial Cell Factories. (2024) https://doi.org/10.1186/s12934-024-02405-1.

[50] H. Gao, J. Zhang, L. Liu, et al., Metagenomic analysis revealing the metabolic role of microbial communities in the free amino acid biosynthesis of Monascus rice vinegar during fermentation, Food Science and Human Wellness. (2024) https://doi.org/10.26599/fshw.2022.9250193.

[51] X. Wang, X. Xu, J. Zhang, et al., Fermentation of Luffa cylindrica by Lactiplantibacillus plantarum P101 enhanced functional properties: Insights into immune modulation, intestinal barrier repair, and intestinal microbiota regulation, Food Bioscience. (2024) https://doi.org/10.1016/j.fbio.2024.104528.

[52]C. Giannone, X. Mess, R. He, et al., How J-chain ensures the assembly of immunoglobulin IgM pentamers, The EMBO Journal. (2024) https://doi.org/10.1038/s44318-024-00317-9.

[53] Y. Li, J. Zheng, Y. Wang, et al., Immuno-stimulatory activity of Astragalus polysaccharides in cyclophosphamide-induced immunosuppressed mice by regulating gut microbiota, Int J Biol Macromol. 242 (2023) 124789. https://doi.org/10.1016/j.ijbiomac.2023.124789.

[54] C.-x. Li, Y. Liu, Y.-z. Zhang, et al., Astragalus polysaccharide: a review of its immunomodulatory effect, Archives of Pharmacal Research. (2022) https://doi.org/10.1007/s12272-022-01393-3.

[55] R. Gao, Z. Wu, W. Dang, et al., Th1/Th2 Immune Imbalance in the Spleen of Mice Induced by Hypobaric Hypoxia Stimulation and Therapeutic Intervention of Astragaloside IV, International Journal of Molecular Sciences. (2025) https://doi.org/10.3390/ijms26062584.

[56] Y. Chen, X. Wei, B. Rui, et al., Probiotic Fermentation of Astragalus membranaceus and Raphani Semen Ameliorates Cyclophosphamide-Induced Immunosuppression Through Intestinal Short-Chain Fatty Acid-Dependent or -Independent Regulation of B Cell Function, Biology. (2025) https://doi.org/10.3390/biology14030312.

[57] V. Horkova, A. Drobek, D. Mueller, et al., Dynamics of the Coreceptor-LCK Interactions during T Cell Development Shape the Self-Reactivity of Peripheral CD4 and CD8 T Cells, Cell Reports. (2020) https://doi.org/10.1016/j.celrep.2020.01.008.

[58] M. Ying, Q. Yu, B. Zheng, et al., Cultured Cordyceps sinensis polysaccharides modulate intestinal mucosal immunity and gut microbiota in cyclophosphamide-treated mice, Carbohydr Polym. 235 (2020) 115957. https://doi.org/10.1016/j.carbpol.2020.115957.

[59] T. Volksdorf, J. Heilmann, S.A. Eming, et al., Tight Junction Proteins Claudin-1 and Occludin Are Important for Cutaneous Wound Healing, Am J Pathol. 187 (2017) 1301-1312. https://doi.org/10.1016/j.ajpath.2017.02.006.

[60] M. Zhang, C. Wu, The relationship between intestinal goblet cells and the immune response, Biosci Rep. 40 (2020) https://doi.org/10.1042/bsr20201471.

[61] Y. Li, Z. Lei, Y. Guo, et al., Fermentation of Ganoderma lucidum and Raphani Semen with a probiotic mixture attenuates cyclophosphamide-induced immunosuppression through microbiota-dependent or -independent regulation of intestinal mucosal barrier and immune responses, Phytomedicine. (2023) https://doi.org/10.1016/j.phymed.2023.155082.

[62] X. Wang, Y. Cao, S. Chen, et al., Anti-Inflammation Activity of Flavones and Their Structure-Activity Relationship, J Agric Food Chem. 69 (2021) 7285-7302. https://doi.org/10.1021/acs.jafc.1c02015.

[63] C. Xie, J. Li, Y. Fang, et al., Proanthocyanins and anthocyanins in chestnut (Castanea mollissima) shell extracts: biotransformation in the simulated gastrointestinal model and interaction with gut microbiota in vitro, J Sci Food Agric. 103 (2023) 3659-3673. https://doi.org/10.1002/jsfa.12480.

[64] G. Zong, R. Deng, Y. Pan, et al., Ginseng polysaccharides ameliorate colorectal tumorigenesis through Lachnospiraceae-mediated immune modulation, Int J Biol Macromol. 307 (2025) 142015. https://doi.org/10.1016/j.ijbiomac.2025.142015.

[65] B. Schiel-Bengelsdorf, P. Dürre, Pathway engineering and synthetic biology using acetogens, FEBS Lett. 586 (2012) 2191-2198. https://doi.org/10.1016/j.febslet.2012.04.043.

[66] Z. Wang, S. Kang, Z. Wu, et al., Muribaculum intestinale restricts Salmonella Typhimurium colonization by converting succinate to propionate, Isme j. 19 (2025) https://doi.org/10.1093/ismejo/wraf069.

[67] Y. Cai, Z. Si, Y. Jiang, et al., Structure-activity relationship of low molecular weight Astragalus membranaceus polysaccharides produced by Bacteroides, Carbohydr Polym. 316 (2023) 121036. https://doi.org/10.1016/j.carbpol.2023.121036.

[68] U. Etxeberria, N. Arias, N. Boqué, et al., Reshaping faecal gut microbiota composition by the intake of trans-resveratrol and quercetin in high-fat sucrose diet-fed rats, J Nutr Biochem. 26 (2015) 651-660. https://doi.org/10.1016/j.jnutbio.2015.01.002.

[69] X. Yan, C. Yang, G. Lin, et al., Antidiabetic Potential of Green Seaweed Enteromorpha prolifera Flavonoids Regulating Insulin Signaling Pathway and Gut Microbiota in Type 2 Diabetic Mice, J Food Sci. 84 (2019) 165-173. https://doi.org/10.1111/1750-3841.14415.